hep-ph/0103123

INLO-PUB 12/00
February 2001

Non-Singlet Structure Functions Beyond the Next-to-Next-to Leading Order

W.L. van Neerven and A. Vogt

Instituut-Lorentz, University of Leiden
P.O. Box 9506, 2300 RA Leiden, The Netherlands

Abstract

We study the evolution of the flavour non-singlet deep-inelastic structure functions $F_{2,\mathrm{NS}}$ and F_3 at the next-to-next-to-next-to-leading order ($\mathrm{N^3LO}$) of massless perturbative QCD. The present information on the corresponding three-loop coefficient functions is used to derive approximate expressions of these quantities which prove completely sufficient for values $x > 10^{-2}$ of the Bjorken variable. The inclusion of the $\mathrm{N^3LO}$ corrections reduces the theoretical uncertainty of α_s determinations from non-singlet scaling violations arising from the truncation of the perturbation series to less than 1%. We also study the predictions of the soft-gluon resummation, of renormalization-scheme optimizations by the principle of minimal sensitivity (PMS) and the effective charge (ECH) method, and of the Padé summation for the structure-function evolution kernels. The PMS, ECH and Padé approaches are found to facilitate a reliable estimate of the corrections beyond $\mathrm{N^3LO}$.

1 Introduction

Structure functions in inclusive deep-inelastic lepton-nucleon scattering (DIS) are among the observables best suited for precise determinations of the strong coupling constant α_s. At present their experimental uncertainties result in an error $\Delta_{\rm exp}\,\alpha_s(M_Z^2) \simeq 0.002$ at the mass of the Z-boson [1]. A further reduction of this error can be expected, especially from measurements at the electron-proton collider HERA after the forthcoming luminosity upgrade. The standard next-to-leading order (NLO) approximation of perturbative QCD summarized in ref. [2], on the other hand, leads to a theoretical error $\Delta_{\rm th}\,\alpha_s(M_Z^2) \approx 0.005$. This error is dominated by the uncertainty due to the truncation of the perturbation series as estimated from the renormalization-scale dependence. Hence calculations beyond NLO are required to make full use of the present and forthcoming data on structure functions.

The ingredients necessary for next-to-next-to-leading order (NNLO) analyses of the structure functions in Bjorken-x space[1] have not been completed up to now: Unlike the two-loop coefficient functions which were calculated some time ago [5] (and completely checked recently [6]), only partial results [7, 8, 9, 10] have been obtained for the three-loop splitting functions so far. However, we have recently demonstrated [11, 12, 13] that the uncertainties resulting from the incompleteness of this information are entirely negligible at $x > 0.05$. Moreover, these uncertainties are small even at much lower x, down to $x \simeq 10^{-4}$ at not too small scales, $Q^2 \gtrsim 10$ GeV^2 [13]. Thus analyses of structure functions in DIS (and of total cross sections for Drell-Yan lepton-pair production [14]) can be promoted to NNLO over a wide kinematic region. Besides more accurate determinations of the parton densities, such analyses facilitate a considerably improved theoretical accuracy $\Delta_{\rm th}\,\alpha_s(M_Z^2) \simeq 0.002$ of the determinations of the strong coupling.

In the present article we extend, for $x > 10^{-2}$, our treatment [11] of the flavour non-singlet (NS) sector dominating α_s-extractions from DIS to the next-to-next-to-next-to-leading order (N^{3}LO). This extension is facilitated by two circumstances: The first is the existence of constraints on the three-loop coefficient functions which prove to be sufficiently restrictive in this region of x. The seven lowest even-integer and odd-integer moments have been computed [7, 8] for the structure function $F_{2,\rm NS}$ in electromagnetic DIS and $F_3^{\nu+\bar{\nu}}$ in charged-current DIS, respectively. Furthermore the four leading large-x terms of these functions are known from the soft-gluon resummation [15, 16]. The second circumstance is the rapid convergence of the splitting-function expansion in the usual $\overline{\rm MS}$ factorization scheme also employed in refs. [7, 8]. Already the impact of the three-loop splitting functions is small at $x > 10^{-2}$, in absolute size (less than 1% on $\alpha_s(M_Z^2)$) as well as compared to the two-loop coefficient functions [11, 12]. Hence one can safely expect that the effect of the unknown four-loop splitting functions on determinations of $\alpha_s(M_Z^2)$ will be well below the 1% accuracy we are aiming at.

[1] See refs. [3, 4] for NNLO analyses based on the integer Mellin-N results of refs. [7, 8] only.

As demonstrated below, the N^{3}LO approximation suffices for achieving this accuracy in the region $x \lesssim 0.75$ usually covered by analyses of DIS data [1]. Terms beyond this order are relevant at $x \gtrsim 0.8$, on the other hand, mainly due to the presence of large soft-gluon logarithms up to $[\ln^{2l-1}(1-x)]/(1-x)$ in the l-loop coefficient functions. The resummation of these logarithms [15, 16] has been extended to the next-to-next-to-leading logarithmic (NNLL) accuracy recently [17]. Here we will study the predictions of this resummation for the factorization-scheme independent ('physical') kernels governing the scaling violations ('evolution') of the non-singlet structure functions. Other approaches to estimate higher-order corrections to these kernels, not restricted to very large x, include Padé summations of the perturbation series [18] as well as renormalization scheme optimizations such as the principle of minimal sensitivity (PMS) [19] and the effective charge (ECH) method [20]. We will also compare these estimates to the full NNLO and N^{3}LO evolution kernels, and investigate the resulting predictions at order α_s^5 (N^{4}LO) and beyond.

The outline of this article is as follows: In section 2 we express the physical evolution kernels, up to N^{4}LO and NNLL accuracy, in terms of the corresponding splitting functions and coefficient functions. The information on the three-loop coefficient functions for $F_{2,\mathrm{NS}}$ and F_3 discussed above is employed in section 3 to derive approximate expressions for their x-dependence. Besides these functions the N^{3}LO evolution kernels also involve convolutions of lower-order coefficient functions for which we provide compact expressions in section 4. These results are put together in section 5 to study the effects of the N^{3}LO terms on the evolution of the structure functions and on the resulting determinations of the strong coupling constant. In section 6 we discuss the predictions of the soft-gluon resummation and of the Padé, PMS and ECH approximations. Finally our results are summarized in section 7. Some relations for the convolutions in section 4 and for the Padé approximations in section 6 can be found in the appendix.

2 Fixed-order and resummed evolution kernels

For the choice $\mu_r^2 = \mu_f^2 = Q^2$ of the renormalization and mass-factorization scales, the structure functions

$$\mathcal{F}_1 = 2F_{1,\rm NS} \;\;, \quad \mathcal{F}_2 = \frac{1}{x} F_{2,\rm NS} \;\;, \quad \mathcal{F}_3 = F_3^{\nu \pm \bar{\nu}} \tag{2.1}$$

are in perturbative QCD given by

$$\begin{aligned} \mathcal{F}_a(x,Q^2) &= \Big[C_a(Q^2) \otimes q_{a,\rm NS}(Q^2)\Big](x) \\ &= \sum_{l=0} a_s^l(Q^2) \Big[c_{a,l} \otimes q_{a,\rm NS}(Q^2)\Big](x) \\ &= \sum_{l=0} a_s^l(Q^2) \int_x^1 \frac{dy}{y}\, c_{a,l}(y)\, q_{a,\rm NS}\left(\frac{x}{y}, Q^2\right) \;. \end{aligned} \tag{2.2}$$

Here $c_{a,l}$ represents the l-loop non-singlet coefficient functions with $c_{a,0}(x) = \delta(1-x)$, and $q_{a,\rm NS}$ stands for the respective combinations of the quark densities. The scale dependence of the running coupling of QCD, in this article normalized as

$$a_s \;\equiv\; \frac{\alpha_s}{4\pi} \;\;, \tag{2.3}$$

is governed by

$$\frac{da_s}{d\ln Q^2} \;=\; \beta(a_s) \;=\; -\sum_{l=0} a_s^{l+2} \beta_l \;\;. \tag{2.4}$$

Besides β_0 and β_1 [2] also the coefficients β_2 and β_3 have been computed [21, 22] in the $\overline{\rm MS}$ renormalization scheme adopted throughout this study. All these four coefficients,

$$\begin{aligned} \beta_0 &= 11 \,-\, 2/3\, N_f \\ \beta_1 &= 102 - 38/3\, N_f \\ \beta_2 &= 2857/2 \,-\, 5033/18\, N_f + \,325/54\, N_f^2 \\ \beta_3 &= 29243.0 - \,6946.30\, N_f + 405.089\, N_f^2 + 1093/729\, N_f^3 \;\;, \end{aligned} \tag{2.5}$$

are required for N^{3}LO calculations. The irrational coefficients in Eq. (2.5) and in Eqs. (2.15) and (2.18) below have been truncated to six digits for brevity. N_f denotes the number of effectively massless flavours (mass effects are not considered in this article). Finally the evolution equations for the parton densities in Eq. (2.2) read

$$\begin{aligned} \frac{d}{d\ln Q^2}\, q_{a,\rm NS}(x,Q^2) &= \Big[P_a(Q^2) \otimes q_{a,\rm NS}(Q^2)\Big](x) \\ &= \sum_{l=0} a_s^{l+1} \Big[P_{a,l} \otimes q_{a,\rm NS}(Q^2)\Big](x) \;\;, \end{aligned} \tag{2.6}$$

where $\otimes$ abbreviates the Mellin convolution written out in the third line of Eq. (2.2). Like the coefficient functions $c_{a,l}(x)$, the $(l+1)$-loop splitting functions $P_{a,l}(x)$ are scale independent for the above choice of μ_r and μ_f.

Explicit expressions up to order α_s^2 can be found in refs. [23] and [5] for the non-singlet splitting functions and coefficient functions, respectively. For the third-order splitting functions $P_{a,2}(x)$ we will employ our approximate expressions of ref. [13]. The three-loop coefficient functions $c_{a,3}(x)$ are the subject of section 3 below.

It is convenient to express the scaling violations of the non-singlet structure functions in terms of these structure functions themselves, thus explicitly eliminating any dependence on the factorization scheme and the scale μ_f. The corresponding 'physical' evolution kernels K_a for $\mu_r^2 = Q^2$ can be derived by differentiating Eq. (2.2) with respect to Q^2 by means of Eqs. (2.4) and (2.6), and finally eliminating $q_{a,\mathrm{NS}}$ using the inverse of Eq. (2.2). Suppressing the dependences on x and Q^2 one arrives at the evolution equations

$$\begin{aligned}
\frac{d}{d\ln Q^2}\mathcal{F}_a &= \left(P_a + \beta\,\frac{d\ln C_a}{da_s}\right)\otimes\mathcal{F}_a \\
&= K_a\otimes\mathcal{F}_a \;=\; \sum_{l=0} a_s^{l+1} K_{a,l}\otimes\mathcal{F}_a \\
&= \left\{a_s P_0 + \sum_{l=1} a_s^{l+1}\left(P_{a,l} - \sum_{k=0}^{l-1}\beta_k \tilde{c}_{a,l-k}\right)\right\}\otimes\mathcal{F}_a
\end{aligned} \tag{2.7}$$

with

$$\begin{aligned}
\tilde{c}_{a,1} &= c_{a,1} \\
\tilde{c}_{a,2} &= 2\,c_{a,2} - c_{a,1}^{\otimes 2} \\
\tilde{c}_{a,3} &= 3\,c_{a,3} - 3\,c_{a,2}\otimes c_{a,1} + c_{a,1}^{\otimes 3} \\
\tilde{c}_{a,4} &= 4\,c_{a,4} - 4\,c_{a,3}\otimes c_{a,1} - 2\,c_{a,2}^{\otimes 2} + 4\,c_{a,2}\otimes c_{a,1}^{\otimes 2} - c_{a,1}^{\otimes 4}\;.
\end{aligned} \tag{2.8}$$

In Eq. (2.8) we have used the abbreviation $f^{\otimes l}$ for the $(l-1)$-fold convolution of a function $f(x)$ with itself, i.e., $f^{\otimes 2} = f\otimes f$ etc. The generalizations $\mathcal{K}_{a,l}$ of the kernels $K_{a,l}$ in Eq. (2.7) to $\mu_r^2 \neq Q^2$ can be obtained by expanding[2] $a_s(Q^2)$ in terms of $a_s(\mu_r^2)$ and $L = \ln(Q^2/\mu_r^2)$, yielding

$$\begin{aligned}
\mathcal{K}_{a,0} &= K_{a,0} \\
\mathcal{K}_{a,1} &= K_{a,1} - \beta_0 L K_{a,0} \\
\mathcal{K}_{a,2} &= K_{a,2} - 2\beta_0 L K_{a,1} - (\beta_1 L - \beta_0^2 L^2)\,K_{a,0} \\
\mathcal{K}_{a,3} &= K_{a,3} - 3\beta_0 L K_{a,2} - (2\beta_1 L - 3\beta_0^2 L^2)\,K_{a,1} \\
&\quad - \left(\beta_2 L - \frac{5}{2}\beta_1\beta_0 L^2 + \beta_0^3 L^3\right) K_{a,0} \\
\mathcal{K}_{a,4} &= K_{a,4} - 4\beta_0 L K_{a,3} - (3\beta_1 L - 6\beta_0^2 L^2)\,K_{a,2} \\
&\quad - (2\beta_2 L - 7\beta_1\beta_0 L^2 + 4\beta_0^3 L^3)\,K_{a,1} \\
&\quad - \left(\beta_3 L - 3\beta_2\beta_0 L^2 - \frac{3}{2}\beta_1^2 L^2 + \frac{13}{3}\beta_1\beta_0^2 L^3 - \beta_0^4 L^4\right) K_{a,0}\;.
\end{aligned} \tag{2.9}$$

[2] Up to the fifth order this expansion can be read off from the $K_{a,0}$ terms of Eq. (2.9).

At N^{m}LO the terms up to $l = m$ are included in Eq (2.7). Hence Eqs. (2.8) and (2.9) formally specify the evolution kernels $\mathcal{K}_a$ up to N^{4}LO. Their extension to higher orders is straightforward but irrelevant for the time being, as at least the coefficient functions beyond four loops will not be calculated in the foreseeable future.

The leading terms of the coefficient functions for $x \to 1$, however, are known to all orders from the soft-gluon resummation [15, 16, 17]. Switching to Mellin moments,

$$f^N \;=\; \int_0^1 dx\, x^{N-1} f(x) \;, \tag{2.10}$$

for the remainder of this section, the large-N (large-x) behaviour of the coefficient functions in Eq. (2.2) takes the form

$$C^N_{\rm res} \;=\; g_0(a_s)\, \exp\Big\{ \ln N\, g_1(\lambda) + g_2(\lambda) + a_s g_3(\lambda) + \mathcal{O}(a_s^2 f(\lambda)) \Big\} \tag{2.11}$$

up to terms which vanish for $N \to \infty$. Here we have used the abbreviation

$$\lambda \;=\; a_s \beta_0 \ln N \;=\; \frac{\alpha_s}{4\pi}\, \beta_0 \ln N \;, \tag{2.12}$$

and we have again put $\mu_r^2 = \mu_f^2 = Q^2$. By virtue of the first line of (2.7), Eq. (2.11) leads to the following expression for the resummed kernel up to next-to-next-to-leading logarithmic (NNLL) accuracy [17]:

$$\begin{aligned} K^N_{\rm res} \;\;=\;\; & -\left(A_1\, a_s + A_2\, a_s^2 + A_3\, a_s^3\right) \ln N \;-\; \left(1 + \frac{\beta_1}{\beta_0} a_s + \frac{\beta_2}{\beta_0} a_s^2\right) \lambda^2 \frac{dg_1}{d\lambda} \\ & - \left(a_s \beta_0 + a_s^2 \beta_1\right) \lambda \frac{dg_2}{d\lambda} \;-\; a_s^2 \beta_0\, \frac{d}{d\lambda}\Big(\lambda g_3(\lambda)\Big) \;+\; \mathcal{O}(a_s^3 (f(\lambda)) \;. \end{aligned} \tag{2.13}$$

Thus the leading logarithmic (LL), next-to-leading logarithmic (NLL) and NNLL large-N contributions to the physical evolution kernels are of the form $(a_s \ln N)^n$, $a_s (a_s \ln N)^n$ and $a_s^2 (a_s \ln N)^n$, respectively. This is in contrast to the coefficient functions which receive contributions up to $(a_s \ln^2 N)^n$. The constants A_l in Eq. (2.13) are the coefficients of the leading [24] large-x terms $1/[1-x]_+$ of the l-loop $\overline{\rm MS}$ splitting functions — recall that

$$f^N \;=\; -\ln N + \mathcal{O}(1) \quad \text{for} \quad f(x) \;=\; 1/[1-x]_+ \;. \tag{2.14}$$

As in Eq. (2.5) inserting the numerical values for the QCD colour factors C_A and C_F, these constants are given by

$$A_1 \;=\; 16/3 \,, \quad A_2 \;=\; 66.4732 - 160/27\, N_f \;, \tag{2.15}$$

and the yet approximate, but sufficiently accurate three-loop result [9, 13]

$$A_3 \;=\; (1178.8 \pm 11.5) - (183.95 \pm 0.85)\, N_f - 64/81\, N_f^2 \;. \tag{2.16}$$

Inserting the explicit form of the functions g_1, g_2 [15] and g_3 [17] in Eq. (2.13) and restoring the dependence on $L = \ln(Q^2/\mu_r^2)$ leads to

$$\begin{aligned}
\mathcal{K}^N_{\rm res} \;=\;& \frac{A_1}{\beta_0}\,\ln(1-\lambda) \;+\; a_s L\,A_1\,\frac{\lambda}{1-\lambda} \;+\; a_s^2 L^2\,A_1\beta_0\,\frac{\lambda(\lambda-2)}{2(1-\lambda)^2} \\
&+ a_s\left\{A_1\beta_1\left(\lambda+\ln(1-\lambda)\right)+(B_1-A_1\gamma_e)\beta_0^2\lambda - A_2\beta_0\lambda\right\}\frac{1}{\beta_0^2(1-\lambda)} \\
&+ a_s^2 L\left\{\left[(B_1-\gamma_e A_1)\beta_0 - A_2\right]\frac{\lambda(\lambda-2)}{(1-\lambda)^2} - A_1\beta_1\,\frac{\ln(1-\lambda)}{\beta_0(1-\lambda)^2}\right\} \\
&+ a_s^2\left\{\left[A_1(\gamma_e^2+\zeta_2)\beta_0^2 + 2A_2\gamma_e\beta_0 + A_3 - 2B_1\gamma_e\beta_0^2 - 2B_2\beta_0\right]\frac{\lambda(\lambda-2)}{2\beta_0(1-\lambda)^2}\right. \\
&\quad + \left[2(A_1\gamma_e - B_1)\beta_1\beta_0^2\,\ln(1-\lambda) + A_1\beta_1^2\left(\lambda^2-\ln^2(1-\lambda)\right)\right. \\
&\qquad \left. - A_1\beta_2\beta_0\,\lambda^2 - A_2\beta_1\beta_0\left(\lambda^2-2\lambda-2\ln(1-\lambda)\right)\right]\frac{1}{2\beta_0^3(1-\lambda)^2} \\
&\quad \left. + 2D_2\frac{\lambda(1-\lambda)}{(1-2\lambda)^2}\right\} \;+\; \mathcal{O}(a_s^3 f(\lambda,L)) \qquad (2.17) \\
\equiv\;& \sum_{l=0}^{\infty} a_s^{l+1}\,\mathcal{K}^N_{{\rm res},l}\;\;.
\end{aligned}$$

Here $\zeta_2 = \pi^2/6$, and γ_e represents the Euler-Mascheroni constant, $\gamma_e \simeq 0.577216$. Furthermore $B_1 = -4$ [15], and the constants B_2 and D_2 are related by [17]

$$B_2 + D_2 \;=\; 36.2657 + 6.34888\,N_f\;\;. \qquad (2.18)$$

We will return to the latter coefficients at the end of the next section.

After subtracting the terms up to order a_s^{m+1} in $\mathcal{K}^N_{\rm res}$ already taken into account in the N^{m}LO terms (2.9), Eq. (2.17) can be added to these fixed-order results to obtain the (N^{m}LO + resummed) approximation for the non-singlet evolution kernels,

$$\mathcal{K}^N_{{\rm N}^m{\rm LO+res}} \;=\; \sum_{l=0}^{m} a_s^{l+1}\,(\mathcal{K}^N_{a,l} - \mathcal{K}^N_{{\rm res},l}) \;+\; \mathcal{K}^N_{\rm res}\;\;. \qquad (2.19)$$

Due to the renormalon singularities at $\lambda = 1$ and $\lambda = 1/2$ in Eq. (2.17) the resummed evolution equations cannot be uniquely inverted to x-space, unlike the fixed-order approximations $\mathcal{K}^N_{a,l}\,\mathcal{F}^N_a$. Note that strength of these singularities — located at $N \simeq 2000$ and $N \simeq 45$ for $\lambda = 1$ and $\lambda = 1/2$, respectively, at $\alpha_s = 0.2$ and $N_f = 4$ — increases with the order of the soft-gluon expansion: the behaviour is logarithmic at the leading-log level, but involves poles of order k for the N^{k}LL approximations. For our numerical study of the all-order case at the end of section 6 we will use the standard 'minimal prescription' contour [27] for the Mellin inversion. This contour runs to the left of the renormalon singularities, but to the right of all other poles in the N-plane.

3 The 3-loop non-singlet coefficient functions

The l-loop coefficient functions $c_{a,l}$ for the non-singlet structure functions $\mathcal{F}_{a=1,2,3}$ defined in Eq. (2.1) can be represented as

$$\begin{aligned} c_{a,l}(x,N_f) &= \sum_{m=0}^{2l-1} A_l^{(m)}\,\mathcal{D}_m \,+\, \tilde{B}_l\,\delta(1-x) \,+\, c_{a,l}^{\,\rm smooth}(x,N_f) \\ &+ \sum_{n=1}^{2l-1} \left(C_{a,l}^{(n)}\,L_1^n + D_{a,l}^{(n)}\,L_0^n \right) \,. \end{aligned} \tag{3.1}$$

Here $A_l^{(m)}$, $\tilde{B}_l$, $C_{a,l}^{(n)}$ and $D_{a,l}^{(n)}$ are numerical coefficients which in general depend on the number of flavours N_f, and we have employed the abbreviations

$$\mathcal{D}_k \,=\, \left[\frac{\ln^k(1-x)}{1-x}\right]_+ , \quad L_1 \,=\, \ln(1-x)\,, \quad L_0 \,=\, \ln x \tag{3.2}$$

for the +-distributions (see Eqs. (3.3) and (3.4) below) and the end-point logarithms. The functions $c_{a,l}^{\,\rm smooth}(x,N_f)$ collect all contributions which are finite for $0 \le x \le 1$. This regular term constitutes the mathematically complicated part of Eq. (3.1), it involves higher transcendental functions like the harmonic polylogarithms introduced in ref. [28]. As usual, the +-distributions are defined via

$$\int_0^1 dx\, a(x)_+ f(x) \,=\, \int_0^1 dx\, a(x)\,\{f(x)-f(1)\} \tag{3.3}$$

where $f(x)$ is a regular function. The convolutions with the distributions occurring in Eq. (3.1) can be written as [3]

$$\begin{aligned} x[\mathcal{D}_k \otimes f](x) &= \int_x^1 dy\, \frac{\ln^k(1-y)}{1-y} \left\{ \frac{x}{y}\, f\!\left(\frac{x}{y}\right) - x f(x) \right\} \\ &+ x f(x) \frac{1}{k+1} \ln^{k+1}(1-x) \,. \end{aligned} \tag{3.4}$$

As already indicated in Eq. (3.1), the coefficients of $\mathcal{D}_m$ and of $\delta(1-x)$ are independent of the choice of the structure function.

The three-loop contributions $c_{S,3}$ known from the soft-gluon resummation read

$$\begin{aligned} c_{S,3}(x,3) &= 512/27\,(\mathcal{D}_5 - L_1^5) - 14400/81\,\mathcal{D}_4 + 264.062\,\mathcal{D}_3 + 1781.704\,\mathcal{D}_2 \\ c_{S,3}(x,4) &= 512/27\,(\mathcal{D}_5 - L_1^5) - 13760/81\,\mathcal{D}_4 + 188.210\,\mathcal{D}_3 + 1962.178\,\mathcal{D}_2 \\ c_{S,3}(x,5) &= 512/27\,(\mathcal{D}_5 - L_1^5) - 13120/81\,\mathcal{D}_4 + 113.938\,\mathcal{D}_3 + 2131.195\,\mathcal{D}_2 \,, \end{aligned} \tag{3.5}$$

where we have again truncated the irrational coefficients and restricted ourselves to the practically relevant cases $N_f = 3$, 4 and 5. Besides the $\mathcal{D}_m$-terms determined in ref. [16],

[3] The second line of Eq. (3.4) is given by $-x f(x) \int_0^x dy\, a(y)$ for a general +-distribution $[a(x)]_+$.

Eq. (3.5) also includes the leading integrable large-x logarithm. The general relation between the coefficients of this term and the leading +-distribution has been conjectured in ref. [29]. Eqs. (3.5) complement the main present constraints on $c_{a,3}(x, N_f)$ provided by the computation [7, 8] of the seven lowest even-integer and odd-integer moments (2.10), respectively, for electromagnetic (e.m.) DIS and the charged-current (CC) combination $F_3^{\nu+\bar{\nu}}$. Note that the coefficients of the leading small-x logarithms are presently unknown here, unlike for the splitting functions and the singlet coefficient functions [10].

We use this information for approximate reconstructions of $c_{2,3}(x, N_f)$ and $c_{3,3}(x, N_f)$ at $N_f = 3$, 4 and 5. Our method is analogous to the treatment of the three-loop splitting functions in refs. [11, 12, 13]: A simple ansatz is chosen for $c_{a,3}^{\rm smooth}$ in Eq. (3.1), and its free parameters are determined from the available moments together with a reasonably balanced subset of the coefficients $A_3^{(0,1)}$, $\tilde{B}_3$, $C_{a,3}^{(n)}$ and $D_{a,3}^{(n)}$. The ansatz for $c_{a,3}^{\rm smooth}$ and the choice of the non-vanishing end-point parameters are then varied in order to estimate the residual uncertainty of $c_{a,3}$. Specifically we keep $A_3^{(1)}$; one of each pair $A_3^{(0)}$ and $\tilde{B}_3$, $C_{a,3}^{(4)}$ and $C_{a,3}^{(3)}$, $C_{a,3}^{(2)}$ and $C_{a,3}^{(1)}$; one or two of the $D_{a,3}^{(n<4)}$; and one or two parameters of a polynomial up to second order in x representing $c_{a,3}^{\rm smooth}$. For a few combinations the resulting system of linear equations which fixes these parameters by the seven moments becomes almost singular, resulting in exceptionally large numerical coefficients. After rejecting those about 5% of the combinations for which the modulus of at least one parameter exceeds 10^5, we are left with about 90 approximations for each case.

Before we present the approximate results for $c_{a,3}(x, N_f)$, it is appropriate to illustrate our procedure by applying it to a known quantity, for which we choose the two-loop e.m. coefficient function $c_{2,2}(x, N_f = 4)$. Adopting the coefficients of $\mathcal{D}_3$ and $\mathcal{D}_2$ defined in Eq. (3.2) from the soft-gluon exponentiation, the procedure described in the preceding paragraph is applied to this function with the small adjustment that two of the $C_{2,2}^{(1,2,3)}$ are kept as $C^{(4)}$ does not occur at two loops according to Eq. (3.1). Also here we reject a couple of combinations, those with parameter(s) of modulus above $3 \cdot 10^3$. The remaining about 70 approximations are compared to the exact result of ref. [5] in Fig. 1.

The seven lowest even-integer moments supplemented by the soft-gluon coefficients $A_2^{(m>1)}$ prove to constrain $c_{2,2}(x)$ rather tightly at $x \gtrsim 0.3$. The region $0.1 \lesssim x \lesssim 0.3$ is less accurately covered, and at $x < 0.1$ the lack of small-x information mentioned above becomes very prominent. Also shown in Fig. 1 is the exact result [5] for $c_{2,2}$ in charged-current DIS. The difference to the electromagnetic case — originating in a sign difference of the contributions from $\gamma/W + q \to q + q + \bar{q}$ with identical quarks in the final-state — is clearly visible only at $x \lesssim 0.2$. The effect of this difference on the evolution of the structure functions at NNLO is unnoticeable at $x \gtrsim 0.1$, and amounts to less that 1% for $x > 0.01$, see Fig. 11 of ref. [11]. We expect that the corresponding three-loop effect will at least not be larger. Hence the approximations for $c_{2,2}(x, N_f)$, constructed for the e.m. case, should be applicable also for neutrino DIS without introducing any relevant error.

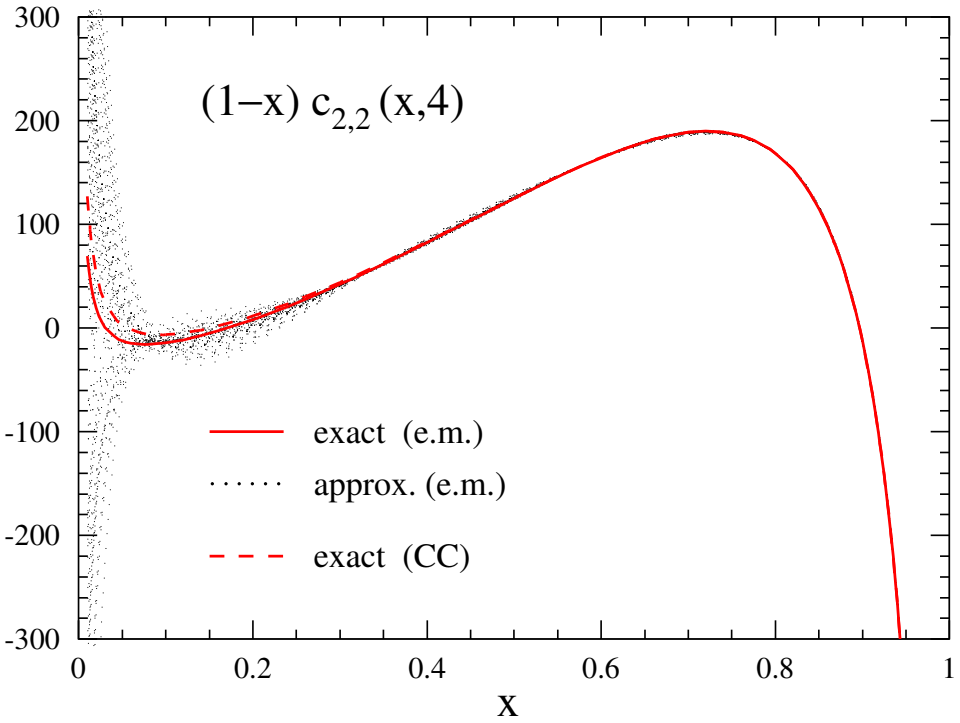

Figure 1: Approximations for the two-loop coefficient functions $c_{2,2}(x, N_f = 4)$ for $F_{2,\mathrm{NS}}^{\mathrm{e.m.}}$ obtained from the lowest seven even-integer moments and the two leading soft-gluon terms, compared to the exact result of ref. [5]. Also shown is the corresponding exact coefficient function for $F_{2,\mathrm{NS}}$ in charged-current DIS.

The corresponding approximations for $c_{2,3}$ and $c_{3,3}$ are shown in Fig. 2 for $N_f = 4$ (concerning the scale of the ordinate recall the rather small expansion parameter (2.3)). As expected, the accuracy pattern is qualitatively similar to the two-loop case of Fig. 2. The uncertainty of $c_{3,3}$ is smaller than that of $c_{2,3}$ at small x, since for $c_{3,3}$ the lowest calculated moment, $N = 1$, is closer to the location of the rightmost pole at $N = 0$. For both functions two representatives, denoted by A and B, are selected which rather completely cover the uncertainty bands. With $c_{S,3}$ of Eq. (3.5) these representatives read

$$\begin{aligned} c_{2,3}^A(x,4) &= c_{S,3}(x,4) - 6456.231\,\mathcal{D}_1 - 1085.97\,\delta(1-x) + 258.876\,L_1^4 \\ &\quad - 22430.79\,L_1 - 74705.15\,x^2 - 4062.14\,(2-x) - 313.0\,L_0^3 \\ c_{2,3}^B(x,4) &= c_{S,3}(x,4) - 5081.227\,\mathcal{D}_1 + 5028.23\,\mathcal{D}_0 + 1059.423\,L_1^4 \\ &\quad - 7292.84\,L_1^2 - 17741.28\,(2-x) - 18154.5\,L_0 + 1168.02\,L_0^3 \end{aligned} \tag{3.6}$$

and

$$\begin{aligned} c_{3,3}^A(x,4) &= c_{S,3}(x,4) - 6940.648\,\mathcal{D}_1 - 1526.23\,\mathcal{D}_0 - 42.598\,L_1^4 \\ &\quad - 33562.64\,L_1 - 91639.87\,x^2 - 5898.84 + 424.49\,L_0^2 \\ c_{3,3}^B(x,4) &= c_{S,3}(x,4) - 4907.988\,\mathcal{D}_1 + 5587.906\,\mathcal{D}_0 + 1092.436\,L_1^4 \\ &\quad - 8267.99\,L_1^2 - 18120.78 - 7083.63\,L_0 + 283.59\,L_0^3 \ . \end{aligned} \tag{3.7}$$

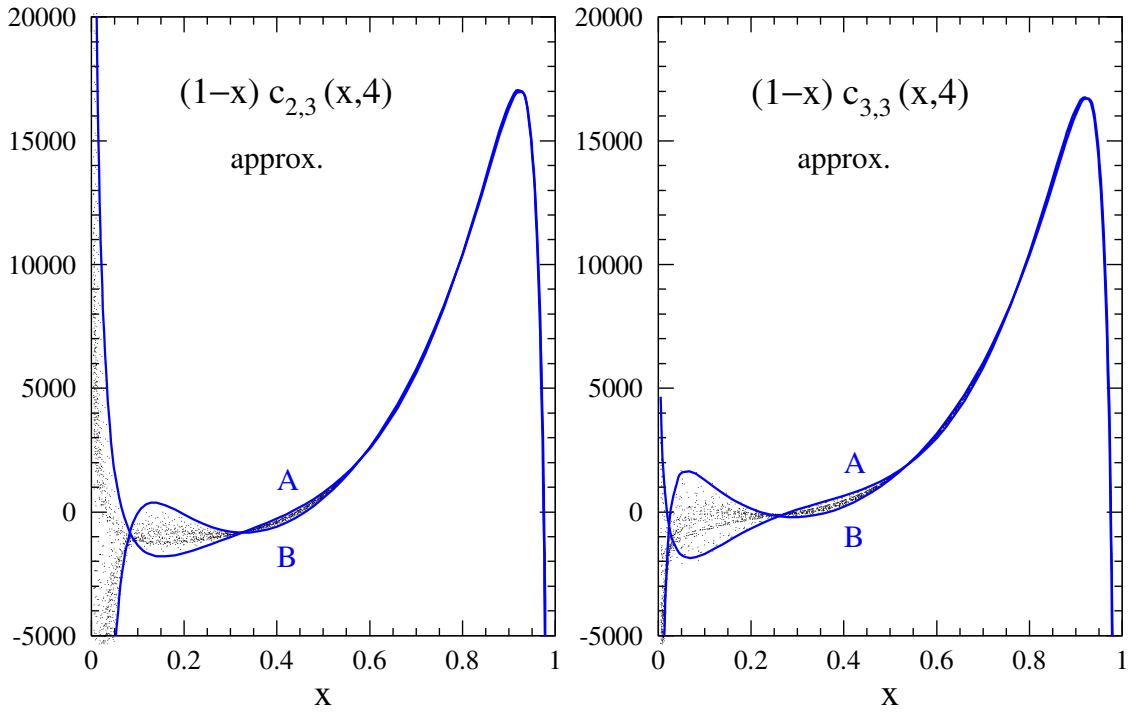

Figure 2: Approximations for the three-loop coefficient functions for $F_{2,\mathrm{NS}}^{\mathrm{e.m.}}$ (left) and the charged-current $F_3^{\nu+\bar{\nu}}$ (right) derived from the respective seven lowest moments [7, 8] and the soft-gluon terms (3.5). The full lines show the selected functions (3.6) and (3.7).

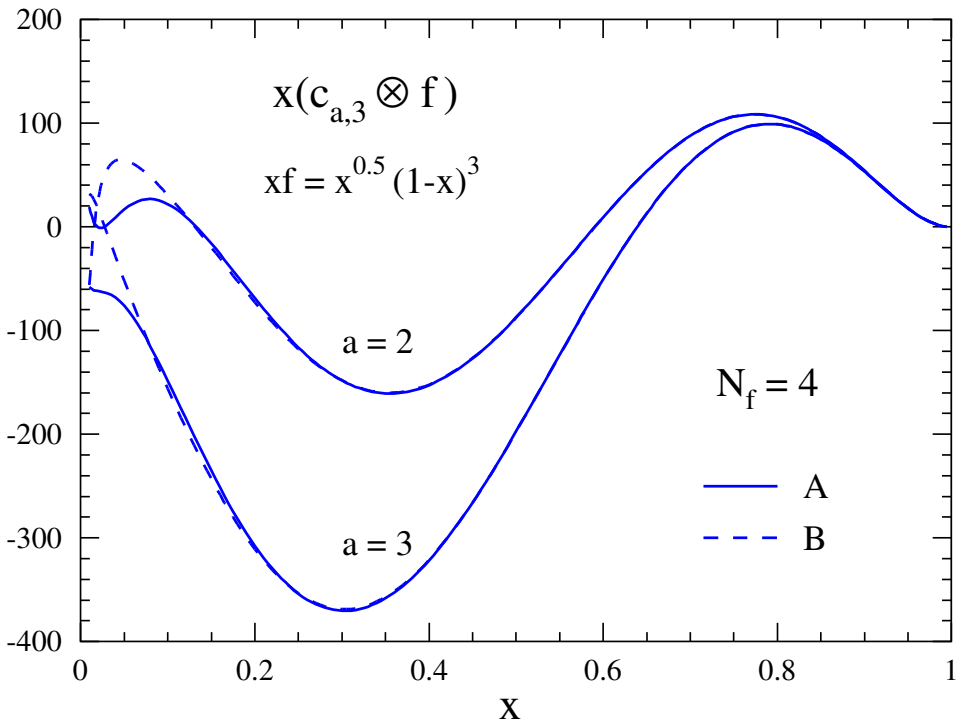

Figure 3: The convolution of the approximations (3.6) and (3.7) selected from the previous figure with a shape typical of hadronic non-singlet distributions.

The uncertainty bands of Fig. 2 do not directly indicate the range of applicability of our approximations, as the coefficient function enter the structure functions and their evolution only via the smoothening convolution (2.2) with non-perturbative initial distributions. In Fig. 3 we therefore present the convolutions of the results (3.6) and (3.7) with a typical non-singlet shape. This illustration shows that the residual uncertainties of $c_{a,3}$ do not lead to any relevant effects for $x \geq 0.1$. The situation at smaller x depends on the numerical size of the $c_{a,3}$ contributions to the evolution kernels given by Eqs. (2.7) and (2.8). Anticipating our findings in section 5, we note that these contributions are actually unproblematically small for $x > 10^{-2}$.

The results for $N_f = 3$ and $N_f = 5$ are similar to those presented in Fig. 2 and Fig. 3. For brevity they are not displayed graphically in this article. The selected approximations for $N_f = 3$ are given by

$$\begin{aligned} c_{2,3}^A(x,3) &= c_{S,3}(x,3) - 6973.782\,\mathcal{D}_1 - 3929.78\,\delta(1-x) + 232.676\,L_1^4 \\ &\quad - 35949.75\,L_1 - 93141.53\,x^2 - 10283.51 - 418.43\,L_0^3 \\ c_{2,3}^B(x,3) &= c_{S,3}(x,3) - 5575.903\,\mathcal{D}_1 + 5474.48\,\mathcal{D}_0 + 927.478\,L_1^4 \\ &\quad - 4646.38\,L_1^2 - 23345.85 - 11094.92\,L_0 + 759.69\,L_0^3 \end{aligned} \tag{3.8}$$

and

$$\begin{aligned} c_{3,3}^A(x,3) &= c_{S,3}(x,3) - 7018.496\,\mathcal{D}_1 - 2957.33\,\delta(1-x) + 162.667\,L_1^4 \\ &\quad - 28363.91\,L_1 - 74640.87\,x^2 - 5720.48\,(1+x) + 330.21\,L_0^2 \\ c_{3,3}^B(x,3) &= c_{S,3}(x,3) - 5160.335\,\mathcal{D}_1 + 6896.360\,\mathcal{D}_0 + 1109.512\,L_1^4 \\ &\quad - 7715.43\,L_1^2 - 20541.22 - 7595.83\,L_0 + 290.34\,L_0^3 \ . \end{aligned} \tag{3.9}$$

The corresponding functions for $N_f = 5$ read

$$\begin{aligned} c_{2,3}^A(x,5) &= c_{S,3}(x,5) - 5951.174\,\mathcal{D}_1 - 391.37\,\mathcal{D}_0 - 2341.422\,L_1^3 \\ &\quad + 19986.58\,L_1 + 5517.39\,(2-x) + 5969.63\,L_0 - 284.23\,L_0^3 \\ c_{2,3}^B(x,5) &= c_{S,3}(x,5) - 4802.695\,\mathcal{D}_1 + 3784.97\,\mathcal{D}_0 + 1041.041\,L_1^4 \\ &\quad - 8021.15\,L_1^2 - 15556.5\,(2-x) - 16445.21\,L_0 + 1084.36\,L_0^3 \end{aligned} \tag{3.10}$$

and

$$\begin{aligned} c_{3,3}^A(x,5) &= c_{S,3}(x,5) - 6560.902\,\mathcal{D}_1 - 2412.54\,\mathcal{D}_0 + 98.499\,L_1^3 \\ &\quad - 27899.69\,L_1 - 82015.71\,x^2 - 2983.82 - 61.43\,L_0^3 \\ c_{3,3}^B(x,5) &= c_{S,3}(x,5) - 4637.854\,\mathcal{D}_1 + 4317.29\,\mathcal{D}_0 + 1070.036\,L_1^4 \\ &\quad - 8767.685\,L_1^2 - 15676.57 - 6543.88\,L_0 + 276.32\,L_0^3 \ . \end{aligned} \tag{3.11}$$

In all cases the average $1/2\,(c_{a,3}^A + c_{a,3}^B)$ represents our central result.

We conclude this section by returning to the coefficients B_2 and D_2 entering the NNLL soft-gluon resummation of the quark coefficient functions (2.11) and structure-function evolution kernels (2.17). If only one of these constants were present, say D_2, then this constant would be fixed by the consistency of Eq. (2.11) with the soft-gluon part $c_{S,2}$ of the NNLO coefficient functions of ref. [5], more precisely by the coefficient $A_2^{(0)}$ in Eq. (3.1). Digressing for a moment, we note that this situation is actually realized for the (very closely related) NNLL soft-gluon resummations of the quark-antiquark annihilation contribution to the Drell-Yan cross section [17] and of the cross section for Higgs production via gluon-gluon fusion in the heavy top-quark limit. For these two processes the NNLO soft- and virtual-gluon contribution have been computed in refs. [25] and [26], respectively. In the present DIS case, however, this consistency conditions only implies the constraint (2.18). An exact result for the coefficient $A_2^{(3)}$ of the three-loop coefficient functions (3.1) would suffice to determine B_2 and D_2, as this coefficient is related to the combination $B_2 + 2D_2$ independent from Eq. (2.18).

As discussed in the paragraph below that of Eq. (3.5), all our approximations (shown for $N_f = 4$ in Fig. 2) include $A_2^{(3)}$. For about 95% of these approximations this coefficient falls into the range

$$A_2^{(3)} \simeq \left\{ \begin{array}{l} -6800 \ldots -5800 \\ -6350 \ldots -5500 \\ -5950 \ldots -5200 \end{array} \right\} \quad \text{for} \quad N_f = \left\{ \begin{array}{l} 3 \\ 4 \\ 5 \end{array} \right\} . \tag{3.12}$$

The comparison of these results to the expansion of Eq. (2.11) (using $g_3(\lambda)$ of ref. [17]) leads to the rather weak constraints

$$B_2 \simeq \left\{ \begin{array}{l} 32 \ldots 87 \\ 42 \ldots 93 \\ 49 \ldots 98 \end{array} \right\} \quad \text{for} \quad N_f = \left\{ \begin{array}{l} 3 \\ 4 \\ 5 \end{array} \right\} \tag{3.13}$$

which can to sufficient accuracy be combined to the estimate

$$B_2 \simeq -P_1^\delta + \frac{1}{3}\,\xi\beta_0 P_0^\delta \quad \text{with} \quad 8 \lesssim \xi \lesssim 12 \; . \tag{3.14}$$

Here P_{l-1}^δ represent the coefficients of $\delta(1-x)$ in the l-loop quark splitting functions. Retaining the colour factors $C_A = N_c = 3$, $C_F = (N_c^2 - 1)/(2N_c)$ these coefficients read

$$\begin{aligned} P_0^\delta &= 3\,C_F \\ P_1^\delta &= C_F^2 \left(\frac{3}{2} + 24\,\zeta_3 - 12\,\zeta_2\right) + C_F C_A \left(\frac{17}{6} - 12\,\zeta_3 + \frac{44}{3}\,\zeta_2\right) \\ &\quad - C_F N_f \left(\frac{1}{3} + \frac{8}{3}\,\zeta_2\right) \end{aligned} \tag{3.15}$$

for our normalization (2.3) of the expansion parameter.

4 Convolutions for the N^{3}LO evolution kernels

Besides the $(l+1)$-loop splitting functions and the l-loop coefficient functions, the N^{l}LO evolution kernels (2.7) involve simple and multiple convolutions of the coefficient functions of lower order. Required at N^{3}LO are the simple and double convolutions of the one-loop coefficient functions $c_{a,1}$ with themselves, $c_{a,1}^{\otimes 2}$ and $c_{a,1}^{\otimes 3}$, and the convolutions of the one- with the two-loop coefficient functions, $c_{a,1} \otimes c_{a,2}$, see Eq. (2.8). Especially the latter lead to rather complex exact expressions. These terms, however, do not require any attention if the evolution is carried out using the moment-space technique [30], as in N-space the convolutions reduce to products. On the other hand, many analyses of data on structure functions are performed using 'brute-force' x-space programs for solving the evolution equations. For application in such programs we provide compact and accurate parametrizations of the convolution contributions to the evolution kernels up to N^{3}LO.

These approximations are derived analogously to those of the two-loop coefficient functions in ref. [11]: The +-distribution parts are treated exactly (truncating irrational coefficients), see the appendix. The integrable $x<1$ terms are fitted to the exact results for $x \geq 10^{-6}$. Finally the coefficients of $\delta(1-x)$ are slightly adjusted from their exact values using the lowest integer moments. The resulting parametrizations deviate from the exact results by no more than a few permille. This accuracy applies directly to Eqs. (4.1)–(4.6) as well as to their convolutions with typical hadronic input distributions.

Using the abbreviations (3.2) the simple convolutions of the one-loop coefficient functions for $F_{2,\rm NS}$ and F_3 can be written as

$$\begin{aligned} c_{2,1}^{\otimes 2}(x) \;=\;& 256/9\,\mathcal{D}_3 - 64\,\mathcal{D}_2 - 283.157\,\mathcal{D}_1 + 304.751\,\mathcal{D}_0 + 346.213\,\delta(1-x) \\ & - 26.51\,L_1^3 + 192.9\,L_1^2 + 198.2\,L_1 + 113.0\,L_1^2 L_0 \\ & - 1.230\,L_0^3 + 9.466\,L_0^2 + 32.45\,L_0 - 483.3\,x - 410.5 \end{aligned} \tag{4.1}$$

and

$$\begin{aligned} c_{3,1}^{\otimes 2}(x) \;=\;& 256/9\,\mathcal{D}_3 - 64\,\mathcal{D}_2 - 283.157\,\mathcal{D}_1 + 304.751\,\mathcal{D}_0 + 345.993\,\delta(1-x) \\ & - 27.09\,L_1^3 + 162.1\,L_1^2 + 248.0\,L_1 + 91.79\,L_1^2 L_0 \\ & - 1.198\,L_0^3 + 3.054\,L_0^2 + 65.54\,L_0 - 305.3\,x - 335.7\ . \end{aligned} \tag{4.2}$$

The corresponding parametrizations for the double convolutions read

$$\begin{aligned} c_{2,1}^{\otimes 3}(x) \;=\;& 1024/9\,\mathcal{D}_5 - 1280/3\,\mathcal{D}_4 - 2757.883\,\mathcal{D}_3 + 9900.585\,\mathcal{D}_2 \\ & + 3917.516\,\mathcal{D}_1 - 12573.13\,\mathcal{D}_0 - 2851.0\,\delta(1-x) \\ & - 151.4\,L_1^5 + 118.9\,L_1^4 - 6155\,L_1^3 - 47990\,L_1^2 - 30080\,L_1 + 6423\,L_1^2 L_0 \\ & - 0.35\,L_0^5 - 4.30\,L_0^4 - 106.7\,L_0^3 - 1257\,L_0^2 - 4345\,L_0 + 3618\,x + 8547 \end{aligned} \tag{4.3}$$

and

$$
\begin{aligned}
c_{3,1}^{\otimes 3}(x) \;=\;& 1024/9\,\mathcal{D}_5 - 1280/3\,\mathcal{D}_4 - 2757.883\,\mathcal{D}_3 + 9900.585\,\mathcal{D}_2 \\
& + 3917.516\,\mathcal{D}_1 - 12573.13\,\mathcal{D}_0 - 2888.1\,\delta(1-x) \\
& - 138.4\,L_1^5 + 409.0\,L_1^4 - 1479\,L_1^3 - 24700\,L_1^2 + 9646\,L_1 - 10080\,L_1^2 L_0 \\
& - 0.119\,L_0^5 + 3.126\,L_0^4 + 84.84\,L_0^3 + 288.7\,L_0^2 + 264.87\,L_0 + 15410\,x + 15890\,.
\end{aligned}
\tag{4.4}
$$

The convolutions $c_{a,2} \otimes c_{a,1}$ for $F_{2,\mathrm{NS}}$ in electromagnetic DIS and for the charged-current combination $F_3^{\nu+\bar{\nu}}$ are parametrized as

$$
\begin{aligned}
&[c_{2,2} \otimes c_{2,1}](x) = \\
&\quad 1536/27\,\mathcal{D}_5 - 343.702\,\mathcal{D}_4 - 633.29\,\mathcal{D}_3 + 5958.86\,\mathcal{D}_2 - 6805.10\,\mathcal{D}_1 - 2464.47\,\mathcal{D}_0 \\
&\quad - 101.7\,L_1^5 - 155.1\,L_1^4 - 6553\,L_1^3 - 23590\,L_1^2 - 10620\,L_1 + 9290\,L_1^2 L_0 - 0.35\,L_0^5 \\
&\quad + 0.64\,L_0^4 + 92.93\,L_0^3 + 761.9\,L_0^2 + 2450\,L_0 - 1251\,x + 6286 + 8609.2\,\delta(1-x) \\
&\quad + N_f \Big\{ 7.0912\,\mathcal{D}_4 - 55.3087\,\mathcal{D}_3 + 18.629\,\mathcal{D}_2 + 619.865\,\mathcal{D}_1 - 584.260\,\mathcal{D}_0 \\
&\quad - 11.71\,L_1^4 + 60.82\,L_1^3 - 618.0\,L_1^2 - 1979\,L_1 - 919.6\,L_1^2 L_0 + 0.48\,L_0^4 \\
&\quad - 1.08\,L_0^3 - 43.83\,L_0^2 - 125.5\,L_0 - 295.1\,x + 522.4\; - 809.14\,\delta(1-x) \Big\}
\end{aligned}
\tag{4.5}
$$

and

$$
\begin{aligned}
&[c_{3,2} \otimes c_{3,1}](x) = \\
&\quad 1536/27\,\mathcal{D}_5 - 343.702\,\mathcal{D}_4 - 633.29\,\mathcal{D}_3 + 5958.86\,\mathcal{D}_2 - 6805.10\,\mathcal{D}_1 - 2464.47\,\mathcal{D}_0 \\
&\quad - 77.39\,L_1^5 + 289.1\,L_1^4 - 2823\,L_1^3 - 12500\,L_1^2 + 25420\,L_1 + 9515\,L_1^2 L_0 - 0.524\,L_0^5 \\
&\quad - 6.104\,L_0^4 + 39.23\,L_0^3 + 553.5\,L_0^2 + 1393\,L_0 + 20080\,x + 2548 + 8478.2\,\delta(1-x) \\
&\quad + N_f \Big\{ 7.0912\,\mathcal{D}_4 - 55.3087\,\mathcal{D}_3 + 18.629\,\mathcal{D}_2 + 619.865\,\mathcal{D}_1 - 584.260\,\mathcal{D}_0 \\
&\quad - 14.30\,L_1^4 + 10.47\,L_1^3 - 775.2\,L_1^2 - 2458\,L_1 - 392.9\,L_1^2 L_0 + 0.482\,L_0^4 \\
&\quad + 2.541\,L_0^3 - 41.04\,L_0^2 - 223.9\,L_0 - 891.9\,x + 468.0\; - 803.43\,\delta(1-x) \Big\}\;.
\end{aligned}
\tag{4.6}
$$

The corresponding results for the charged-current quantities $F_{2,\mathrm{NS}}$ and $F_3^{\nu-\bar{\nu}}$ are obtained by replacing the second and third line of Eqs. (4.5) and (4.6), respectively, by

$$
\begin{aligned}
&- 109.2\,L_1^5 - 243.4\,L_1^4 - 6890\,L_1^3 - 24000\,L_1^2 + 10840\,L_1 + 9144\,L_1^2 L_0 - 0.45\,L_0^5 \\
&+ 1.80\,L_0^4 + 114.0\,L_0^3 + 856.6\,L_0^2 + 2602\,L_0 - 711.6\,x + 6298 + 8569.2\,\delta(1-x)
\end{aligned}
$$

and

$$
\begin{aligned}
&- 77.39\,L_1^5 + 295.5\,L_1^4 - 2587\,L_1^3 - 10580\,L_1^2 + 30580\,L_1 + 6461\,L_1^2 L_0 - 0.404\,L_0^5 \\
&- 5.525\,L_0^4 + 23.80\,L_0^3 + 484.7\,L_0^2 + 1577\,L_0 + 22220\,x + 3349 + 8485.0\,\delta(1-x)\;.
\end{aligned}
$$

5 Numerical results for the scaling violations

In this section we illustrate the effect of the next-to-next-to-next-to-leading order ($\mathrm{N^3LO}$) contributions to the physical evolution kernels (2.7)–(2.9) for the electromagnetic structure function $F_{2,\mathrm{NS}}$ and the charged-current combination $F_3^{\nu+\bar{\nu}}$ henceforth simply denoted F_3. Specifically, we will discuss the logarithmic derivatives $\dot{F}_a \equiv d\ln F_a/d\ln Q^2$ calculated at a fixed reference scale $Q^2 = Q_0^2$ for the initial conditions

$$F_{2,\mathrm{NS}}(x,Q_0^2) \;=\; xF_3(x,Q_0^2) \;=\; x^{0.5}(1-x)^3 \;\; . \tag{5.1}$$

The simple model shape (5.1) incorporates the most important features of non-singlet x-distributions of nucleons. Its overall normalization is irrelevant for the logarithmic derivatives considered here. The reference scale Q_0^2 is specified via

$$\alpha_s(\mu_r^2{=}Q_0^2) \;=\; 0.2 \tag{5.2}$$

irrespective of the order of the expansion. Eq. (5.2) corresponds to $Q_0^2 \simeq 30$ GeV^2, a scale typical for fixed-target DIS, for $\alpha_s(M_Z^2) \simeq 0.116$ beyond leading order (LO). The same input (5.1) and (5.2) is chosen at all orders and for both structure functions in order to facilitate a direct comparison of the various contributions to the evolution kernels (2.7). All graphical illustrations below refer to $N_f = 4$ effectively massless quark flavours.

Before turning to the numerical results we have to specify our treatment of the four-loop splitting functions $P_{a,3}$. These functions enter Eq. (2.7) at order α_s^4 ($\mathrm{N^3LO}$) together with the three-loop coefficient functions (3.6) – (3.11) and the convolutions (4.3) – (4.6). As already mentioned in the introduction, the size of the two- and three-loop terms in the expansion of the non-singlet splitting functions strongly indicates that the effects of $P_{a,3}$ are very small in the x-region addressed by the present study, $x > 10^{-2}$. Hence a rather rough estimate of these quantities is sufficient here. We have checked that the [0/1] Pade approximation[4] gives a reasonable, though not particularly accurate estimate of the three-loop non-singlet splitting functions $P_{a,2}^N$ in N-space for $N_f = 3\ldots5$. Thus we choose the Mellin inverse of

$$P_{a,3}^N \;\simeq\; \eta\,[P_{a,3}^N]_{\,[1/1]\,\text{Padé}} \;\; , \quad \eta \;=\; 0 \;\ldots\; 2 \tag{5.3}$$

as our estimate of $P_{a,3}(x)$, i.e., we assign a 100% error to the predictions of the [1/1] Padé summation (the [0/2] Padé results are similar). The results obtained by combining Eq. (5.3) for $\eta = 2$ with $c_{a,3}^A$ in Eqs. (3.6) – (3.11) are denoted by $\mathrm{N^3LO}_A$ in the figures below, those using $\eta = 0$ and $c_{a,3}^B$ by $\mathrm{N^3LO}_B$. As in section 3 the central predictions $1/2\,(\mathrm{N^3LO}_A + \mathrm{N^3LO}_B)$ are not shown separately.

The logarithmic scale derivatives $\dot{F}_{2,\mathrm{NS}}$ and $\dot{F}_3$ resulting from Eqs. (5.1), (5.2) are shown in the left parts of Fig. 4 and Fig. 5, respectively, for the standard choice $\mu_r^2 = Q^2$

[4] A brief discussion of the Padé summations and the resulting higher-order approximations can be found in the next section.

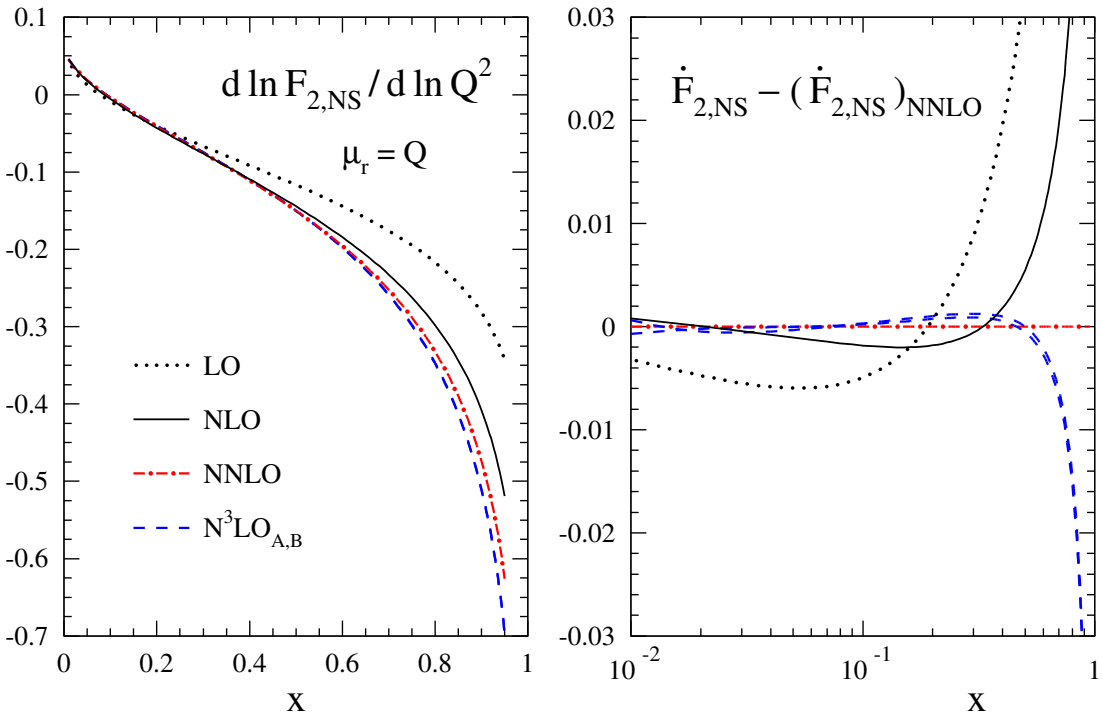

Figure 4: The perturbative expansion of the scale derivative $\dot{F}_{2,\mathrm{NS}} \equiv d\ln F_{2,\mathrm{NS}}/d\ln Q^2$ of the electromagnetic structure function $F_{2,\mathrm{NS}}$ at $\mu_r^2 = Q^2 \simeq 30$ GeV^2 for the initial conditions specified in Eqs. (5.1) and (5.2). The differences between the predictions at different orders in α_s are shown on a larger scale in the right part.

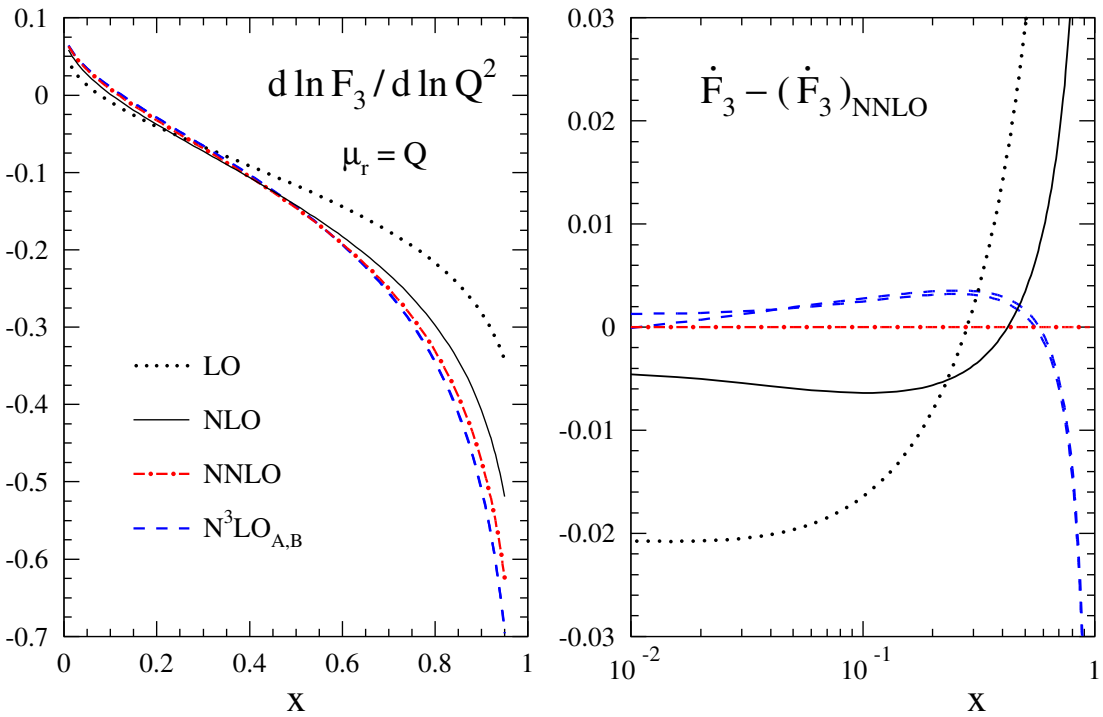

Figure 5: As Fig. 4, but for the charged-current combination $F_3 \equiv F_3^{\nu+\bar{\nu}}$. In all figures the subscripts A and B at N^{3}LO refer to the approximations discussed below Eq. (5.3).

of the renormalization scale. At $x \lesssim 0.5$ the size of the NNLO and N^{3}LO corrections can barely be read on the scale of these graphs, therefore the differences $\dot{F}_a - (\dot{F}_a)_{\rm NNLO}$ are displayed on a larger scale in the left parts of both figures. The difference of the N^{3}LO$_A$ and N^{3}LO$_B$ results is very small down to $x \simeq 10^{-2}$ even on this enlarged scale, demonstrating that our approximations (3.6) – (3.11) and (5.3) are completely sufficient in this region of x. For both structure functions the N^{3}LO corrections are large only at very large x, where the kernels are dominated by the universal soft-gluon contributions. Towards smaller x the N^{3}LO effects rapidly decrease, e.g., from 6% at $x = 0.85$ to 2% at $x = 0.65$. The corresponding NNLO contributions amount to about 12% and 6%, respectively. At $10^{-2} \lesssim x \lesssim 0.6$ the N^{3}LO corrections are particularly small for $F_{2,\rm NS}$.

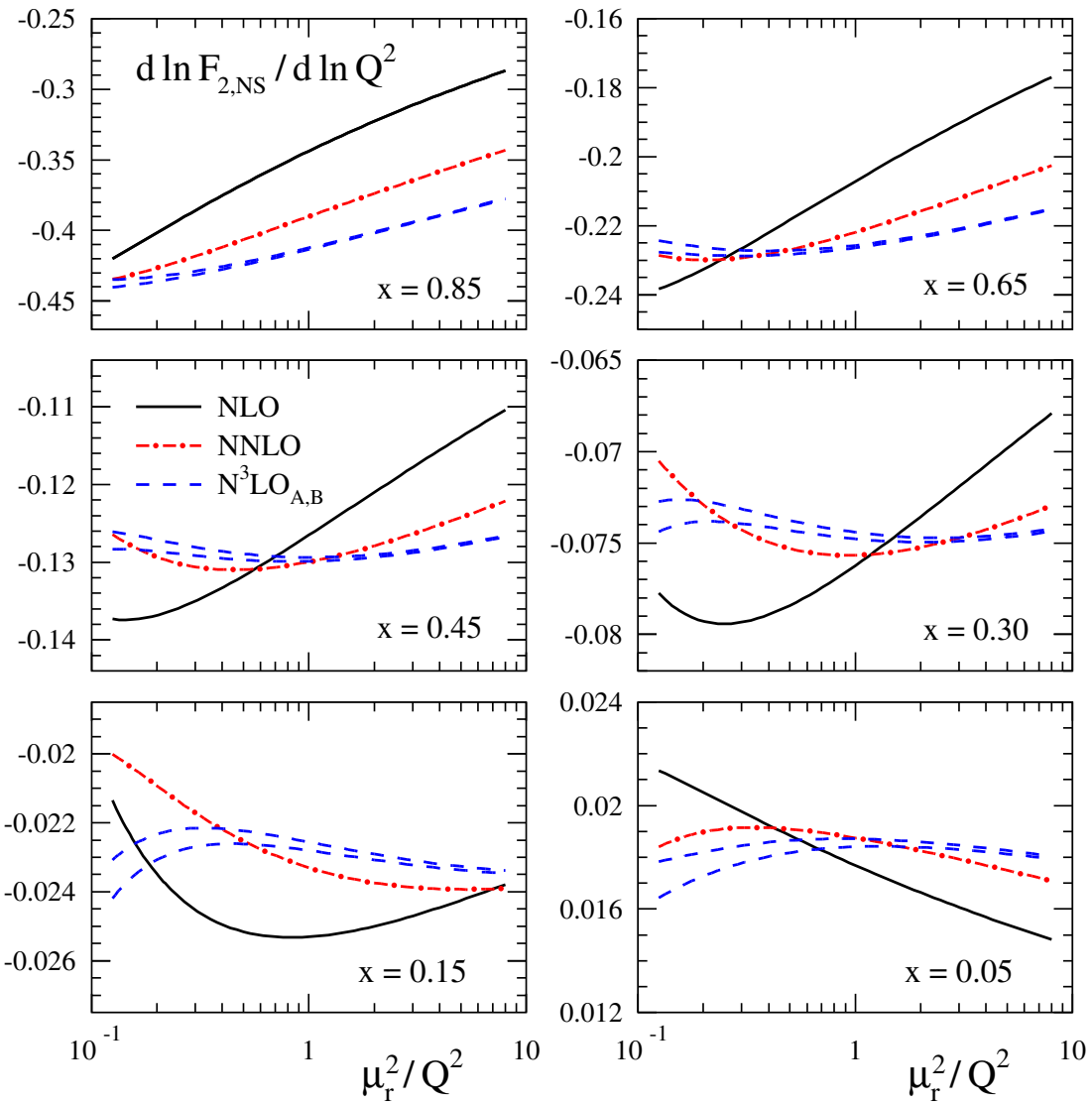

Figure 6: The dependence of the NLO, NNLO and N^{3}LO predictions for $d \ln F_{2,\rm NS}/d \ln Q^2$ at $Q^2 = Q_0^2 \simeq 30$ GeV^2 on the renormalization scale μ_r for six typical values of x.

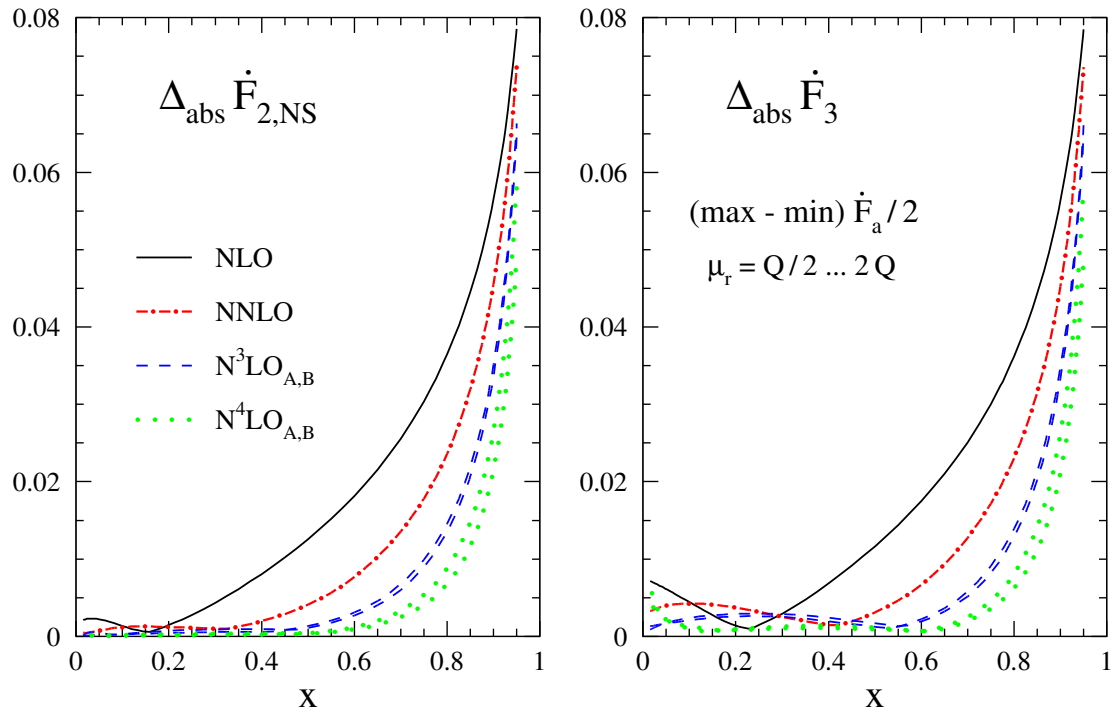

Figure 7: The renormalization scale uncertainties, as estimated by the quantities $\Delta_{\rm abs}\dot{F}_a$ defined in Eq. (5.4), of the perturbative predictions for the scale derivatives of $F_{2,NS}$ and F_3 displayed in Fig. 4 and Fig. 5, respectively. Also included are the corresponding approximate N^{4}LO results derived in section 6 below.

The dependence of these scale derivatives on the renormalization scale[5] is illustrated in Fig. 6 and Fig. 7. In the former figure the consequences of varying μ_r are shown for $\dot{F}_{2,\rm NS}$ at six representative values of x (note that the scales of the ordinates are different in all six parts). Here we vary μ_r over a rather wide range, $\frac{1}{8}\,Q^2 \le \mu_r^2 \le 8Q^2$, corresponding to $0.29 \gtrsim \alpha_s(\mu_r^2) \gtrsim 0.15$ for the initial condition (5.2). In the latter figure we display the absolute scale uncertainties of $\dot{F}_{2,\rm NS}$ and $\dot{F}_3$ at $Q^2 = Q_0^2$, estimated by

$$\Delta_{\rm abs}\dot{F}_a \;\equiv\; \frac{1}{2}\left\{\max\left[\dot{F}_a(\mu_r^2 = \frac{1}{4}\,Q^2 \ldots 4Q^2)\right] - \min\left[\dot{F}_a(\mu_r^2 = \frac{1}{4}\,Q^2 \ldots 4Q^2)\right]\right\} \;, \qquad (5.4)$$

i.e., using the smaller conventional interval $\frac{1}{2}\,Q \ldots 2\,Q$ for μ_r. Also shown here are the further improvements resulting from including the approximate α_s^5 (N^{4}LO) contributions to Eqs. (2.7) – (2.9) discussed in the next section.

Our new N^{3}LO results represent a clear improvement over the NNLO stability [11] for all x-values of Fig. 6 except for $x = 0.05$ (here, however, the absolute spread is very small, see Fig. 7), where the difference between the N^{3}LO$_A$ and N^{3}LO$_B$ results at small μ_r becomes comparable to the μ_r-variation at NNLO. This enhanced sensitivity at small scales is due to the larger values of α_s up to almost 0.3, which enter the approximate contributions to Eq. (2.7) as α_s^4. The present approximation uncertainties of the N^{3}LO results are

[5] As already mentioned below Eq. (2.4), we use the $\overline{\rm MS}$ renormalization scheme throughout this study.

actually dominated by the estimate (5.3) for the four-loop splitting functions, not by the residual uncertainties of the three-loop coefficient functions quantified in Eqs. (3.6)–(3.11).

The results shown in Fig. 7 correspond to relative uncertainties $(\Delta_{\rm abs}\dot{F}_a)/\dot{F}_a$ of 8% at NNLO and 5% and 3% at N^{3}LO and N^{4}LO, respectively, for both $F_{2,\rm NS}$ and F_3 at $x = 0.85$. The corresponding figures at $x = 0.65$ read 5% (NNLO), 2% (N^{3}LO) and 1% (N^{4}LO). These scale uncertainties are rather similar to the relative size of the highest-order contributions at $\mu_r^2 = Q^2$ in Fig. 4 and Fig. 5 (for the N^{4}LO contribution see Fig. 11 in section 6). Hence the μ_r-variation (5.4) and the size of the last contribution included in Eq. (2.7) yield consistent uncertainty estimates in this region of x. At smaller x the absolute scale uncertainties are very small at N^{3}LO and N^{4}LO. For $\Delta_{\rm abs}\dot{F}_{2,\rm NS}$ values even below 0.001 are reached for $x \leq 0.5$ at N^{3}LO and $x \leq 0.6$ at N^{4}LO.

We conclude this section by illustrating the effect of the higher-order terms in Eq. (2.7) on the determination of α_s from the scaling violations of non-singlet structure functions. For this illustration we assume that $F_{2,\rm NS}$ and F_3 at $Q_0^2 \simeq 30$ GeV^2 are given by Eq. (5.1) with negligible uncertainty. The resulting average N^{3}LO predictions of $\dot{F}_{2,\rm NS}$ and $\dot{F}_3$ for $\mu_r^2 = Q_0^2$ and $\alpha_s = 0.2$ are employed as model data at $x_k = 0.1\,k - 0.05$ with $k = 1, \ldots, 8$. Roughly following the experimental pattern, we assign errors of 0.005 for $k = 2, \ldots 6$, of 0.01 for $k = 1, 7$ and of 0.02 for $k = 8$ to these data points (for Eq. (5.5) only the relative size of these errors is relevant). Again already including the N^{4}LO estimate obtained in the next section, the fits of $\alpha_s(Q_0^2)$ to these model data yield

$$\begin{aligned}
\alpha_s(Q_0^2)_{\rm NLO} &= 0.2080\ {}^{+\,0.021}_{-\,0.013}\ , \quad 0.2035\ {}^{+\,0.019}_{-\,0.011} \\
\alpha_s(Q_0^2)_{\rm NNLO} &= 0.2010\ {}^{+\,0.008}_{-\,0.0025}\ , \quad 0.1995\ {}^{+\,0.0065}_{-\,0.0015} \\
\alpha_s(Q_0^2)_{\rm N^3LO} &= 0.2000\ {}^{+\,0.003}_{-\,0.001}\ , \quad 0.2000\ {}^{+\,0.0025}_{-\,0.0005} \\
\alpha_s(Q_0^2)_{\rm N^4LO} &= 0.2000\ {}^{+\,0.0015}_{-\,0.0005}\ , \quad 0.2005\ {}^{+\,0.0015}_{-\,0.0005}
\end{aligned} \tag{5.5}$$

where the first column refers to $F_{2,\rm NS}$ and the second to F_3. The central values represent the respective results for $\mu_r^2 = Q_0^2$, and the errors are due to the renormalization scale variation $\frac{1}{4}\,Q^2 \leq \mu_r^2 \leq 4\,Q^2$, for the N^{3}LO and N^{4}LO cases combined with the approximation uncertainties. Unlike the NNLO terms, the N^{3}LO and N^{4}LO corrections do not cause significant shifts of the central values, but just lead to a reduction of the μ_r uncertainties which reach about $\pm 1\%$ at N^{3}LO. The difference of the NLO and NNLO central results for F_3 is half as large as that for $F_{2,\rm NS}$. This effect is due to larger positive corrections to the logarithmic derivative at $x < 0.4$ in the former case (see Figs. 4 and 5), which counteract the effect of the negative corrections at large x in the fit. As far as Eq. (5.5) can be compared to the fits of real data in refs. [3, 4] (where higher-twist contributions affecting the central values are included), our finding are consistent with those results.

6 Resummations and optimizations

Finally we address the predictions of the soft-gluon resummation, the ECH and PMS scheme optimizations, and the Padé approximations for the physical evolution kernel K_a in Eq. (2.7). Being especially interested in the region of large-x / large-N, where the higher-order corrections are large but similar for $F_{2,\rm NS}$ and F_3, we will for brevity focus on the former, more accurately measured quantity. Also in this section the numerical results are given for $N_f = 4$ and the initial conditions (5.1) and (5.2). We will mainly consider the predictions of the above-mentioned approaches at fixed order in α_s, and only at the end briefly turn to the all-order results for the soft-gluon exponentiation and the Padé summations.

The N^{l}LO predictions of the soft-gluon resummation for the kernels (2.7) are given by the terms $a_s^{l+1}\mathcal{K}_{{\rm res},l}$ in Eq. (2.17). Recall that the leading logarithmic (LL), next-to-leading logarithmic (NLL) and next-to-next-to-leading logarithmic (NNLL) contributions behave as $\ln^{l+1}N$, $\ln^l N$ and (at $l \geq 2$) $\ln^{l-1}N$, respectively. The terms in the l-loop coefficient functions $c_{a,l}$ proportional to $\ln^k N$ with $k = l+2, \ldots, 2l$ cancel in the combinations (2.8) for $l \geq 2$. This implies that, from $l = 5$ onwards, actually none of the four leading $\ln^k N$ terms of $c_{a,l}$ presently fixed by the soft-gluon exponentiation (2.11) contributes to the N^{l}LO kernels (2.7). Consequently, we expect a pattern for the numerical soft-gluon approximations to the physical kernels which is rather different from that discussed in ref. [16] for the $\overline{\rm MS}$ coefficient functions.

The cumulative effect of soft-gluon terms at NNLO (α_s^3) and N^{3}LO (α_s^4) is compared to the (approximate) full results in Fig. 8. The two solid curves in the right plot refer to the N^{3}LO$_A$ and N^{3}LO$_B$ approximation discussed below Eq. (5.3), the two NNLL results to $\xi = 8$ and $\xi = 12$ in Eq. (3.14). For the (undisplayed) NLO contribution the LL and NNLL predictions are considerably smaller and larger, respectively, than the full result, whereas the inclusion of also the $a_s^2 N^0$ term arising from soft and virtual emissions leads to a reasonable approximation. Combined with this situation, the results of Fig. 8 indicate that the number of soft-gluon logarithms required for a realistic approximation at N^{l}LO systematically increases with the order l: The full NLO, NNLO, and N^{3}LO curves run between the LL and NLL, close to the NLL, and between the NLL and NNLL results, respectively. The NNLL soft-gluon contribution may thus be expected to represent a reasonable estimate for the N^{4}LO (α_s^5) term of Eq. (2.7) at large x / large N. As shown in Fig. 9 [6], however, the spread due to the present uncertainty (3.14) of the parameters B_2 and D_2 entering Eq. (2.17) is unfortunately rather large. Moreover, even if with this uncertainty removed, e.g., by a future exact calculation of the three-loop coefficient functions, Figs. 8 and 9 indicate that the soft-gluon resummation can hardly be expected to provide accurate information on the N^{4}LO term, even for moments as large as $N \simeq 30$.

[6] Already Fig. 3 demonstrates that the universal soft-gluon terms do not provide a good approximation for $x < 0.7$, hence the corresponding x-space results in Figs. 9 and 12 are shown only at larger x.

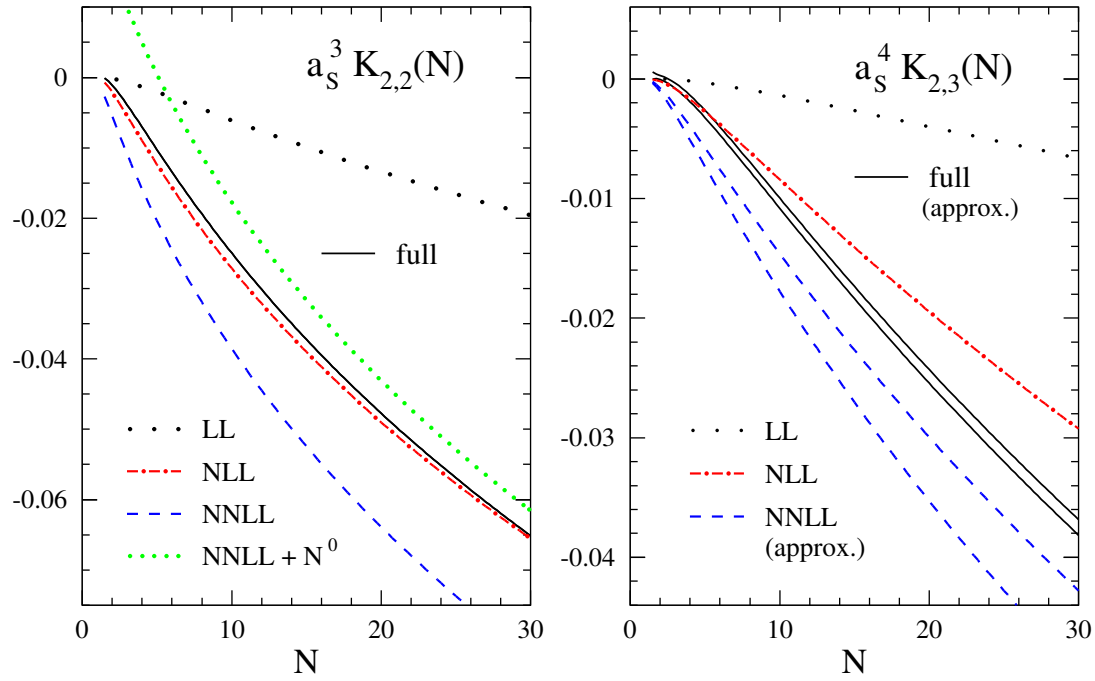

Figure 8: The successive soft-gluon approximations for the NNLO (left) and N^{3}LO (right) contributions to the moments (2.10) of the evolution kernel (2.7) at $\mu_r^2 = Q^2$, compared with the full results for $F_{2,\rm NS}$ addressed in the previous section. Besides the $\ln^n N$ terms of $K_{\rm res,2}$ in Eq. (2.17), also the N^0 contribution is included for the NNLO case.

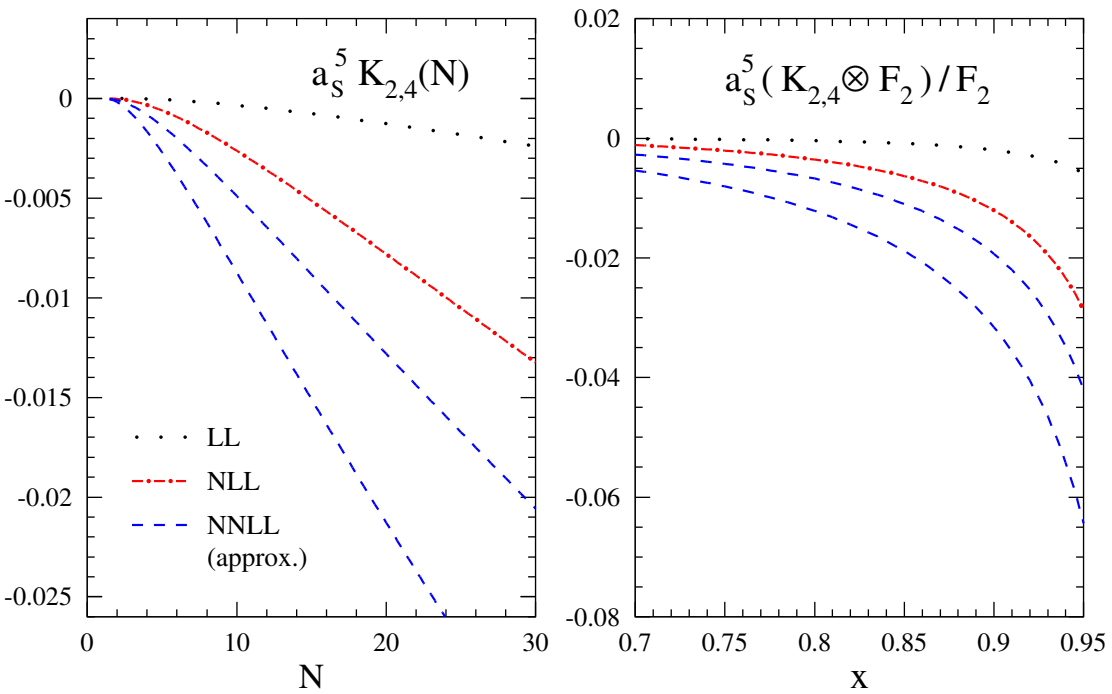

Figure 9: The results of the soft-gluon resummation (2.17) for the N^{4}LO contribution to the kernel (2.7). The left part corresponds to the right plot of Fig. 8, in the right part the resulting large-x predictions are shown for the α_s^5 corrections to the results of Fig. 4.

The renormalization-scheme optimizations assume that that the higher-order corrections to the N^{l}LO physical kernels $\mathcal{K}_a^{(l)N}$ in N-space given by

$$\frac{d \ln \mathcal{F}_a^N}{d \ln Q^2} \;=\; \mathcal{K}_a^{(l)N} \;=\; a_s K_0^N \left(1 + a_s r_{a,1}^N + \ldots + a_s^l r_{a,l}^N\right) \tag{6.1}$$

are small in a certain 'optimal' scheme. The principle of minimal sensitivity (PMS) proposed in ref. [19] selects this scheme by the requirement

$$\frac{d\, \mathcal{K}_a^N(\mathrm{RS})}{d(\mathrm{RS})} \;=\; 0 \;, \tag{6.2}$$

where $d/d(\mathrm{RS})$ abbreviates the derivatives with respect to the l independent parameters specifying the renormalization scheme at N^{l}LO. In the effective charge (ECH) method of ref. [20], on the other hand, these parameters are chosen such that

$$r_{a,1}^N \;=\; \ldots \;=\; r_{a,l}^N \;=\; 0 \;. \tag{6.3}$$

Assuming that in these schemes the next terms $r_{a,l+1}^N$ are not just small but vanishing, the transformation back to $\overline{\mathrm{MS}}$ (or any other scheme) leads to the respective PMS and ECH predictions for this quantity in terms of $r_{a,1}^N \;\ldots\; r_{a,l}^N$ and the coefficients (2.4) of the β-function. Up to r_4 these predictions are explictly given in Eqs. (6) – (11) and (13) – (17) of ref. [31], thus we refrain from repeating them here.

Another approach for estimating the higher-order corrections is provided by the Padé summation of the perturbation series, for QCD in detail discussed, e.g., in refs. [18]. In this method $\mathcal{K}_a^{(l)N}$ in Eq. (6.1) is replaced by

$$\mathcal{K}_{a,\,[\mathcal{N}/\mathcal{D}]}^N \;=\; a_s K_0 \, \frac{1 + a_s p_{a,1}^N + \ldots + a_s^{\mathcal{N}} p_{a,\mathcal{N}}^N}{1 + a_s q_{a,1}^N + \ldots + a_s^{\mathcal{D}} q_{a,\mathcal{D}}^N} \tag{6.4}$$

with

$$\mathcal{D} \;\geq\; 1 \quad \text{and} \quad \mathcal{N} + \mathcal{D} \;=\; l \;. \tag{6.5}$$

The determination of the parameters p_i and q_j from the $r_1 \;\ldots\; r_l$ of Eq. (6.1) are automatized in programs for symbolic manipulation such as MAPLE [32]. Expanding $\mathcal{K}_{a,\,[\mathcal{N}/\mathcal{D}]}^N$ to order $l+1$ then yields the $[\mathcal{N}/\mathcal{D}]$ Padé predictions for the N^{l+1}LO coefficients $r_{a,l+1}^N$. Also these predictions need not to be written down here. Beyond the second-order results there is no obvious relation between the predictions of the scheme optimizations and those of the Padé approximations. Consistent result of these methods for $r_{l>2}$ are thus usually considered as evidence of the approximate correctness of these predictions [18].

The PMS, ECH and Padé results for the NNLO and N^{3}LO N-space kernels (6.1) are compared in Fig. 10 to the (approximate) full results already shown, on the same scale, in Fig. 8. Disregarding large relative, but small absolute deviations at NNLO for small N, the PMS and ECH results (which are very similar at NNLO and identical at N^{3}LO)

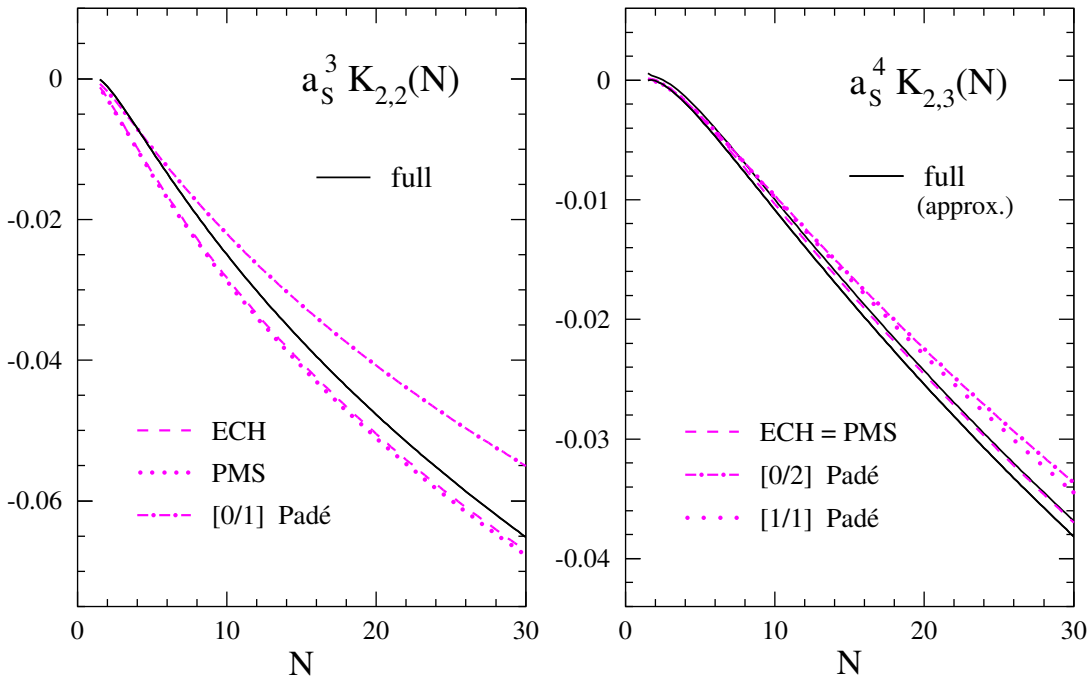

Figure 10: The PMS, ECH and Padé estimates of the NNLO (left) and N^{3}LO (right) parts of the N-space evolution kernel for $F_{2,\rm NS}$ at $\mu_r^2 = Q^2$, compared with the full results illustrated in x-space in section 5. The scales of the graphs are the same as in Fig. 8.

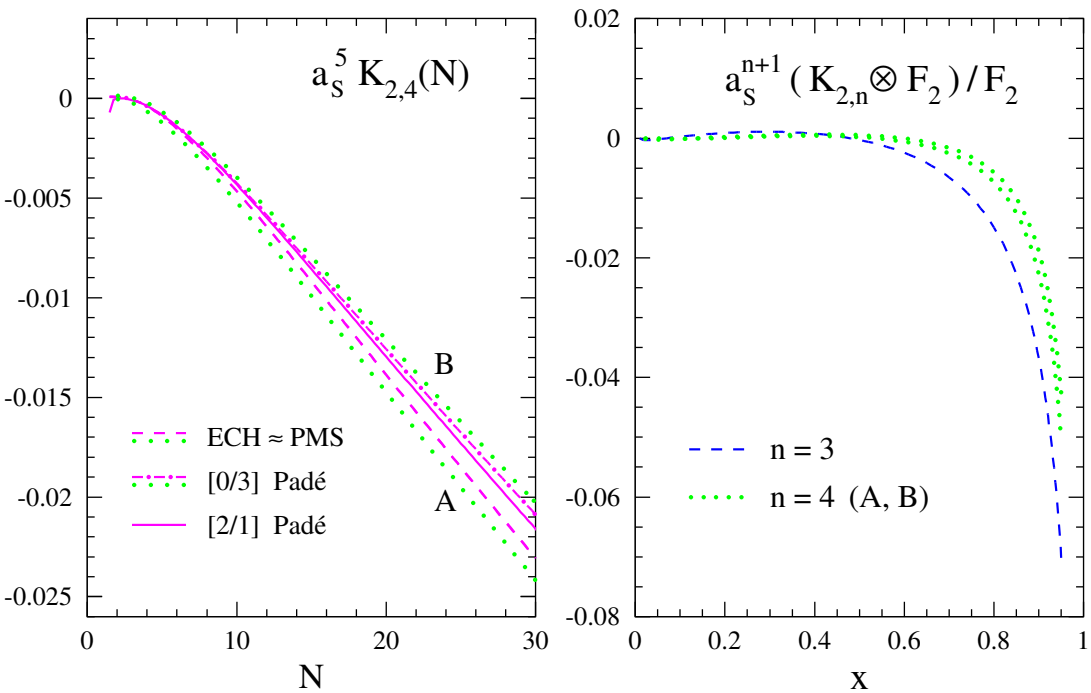

Figure 11: The PMS, ECH and Padé estimates of the N^{4}LO contributions to the evolution kernel (2.7) for $F_{2,\rm NS}$. The left part is analogous to Fig. 10, in the right part the resulting α_s^5 corrections to the result in Fig. 4 are compared to the α_s^4 (N^{3}LO) contribution. The scales of the graphs are the same as in Fig. 9.

represent good approximations at both orders. The Padé approximations are somewhat smaller, however, this offset seems to decrease with the order in α_s. In the left part of Fig. 11 we present the corresponding N^{4}LO predictions. The inner three curves have been derived from the central N^{3}LO results of section 5. The PMS and ECH are again very similar, they are not shown separately. The impact of the present uncertainty of the N^{3}LO kernels, dominated by the estimate (5.3) of the four-loop splitting functions, is included in the two dotted curves which represent our final estimate for the N^{4}LO term and its uncertainty. In the right part of Fig. 10 the N^{4}LO corrections to the results of Fig. 4 are compared to the N^{3}LO contribution. Within the large uncertainties of the latter, these results are consistent with the NNLL soft-gluon prediction shown in Fig. 9. The consequences of including the N^{4}LO estimates have been presented in Fig. 7 and Eq. (5.5), respectively, for the renormalization-scale stability and the determination of α_s.

Finally the $\alpha_s^{l>5}$ infinite-order predictions of the soft-gluon resummation (2.17) (using the minimal prescription contour [27]) and the Padé approximations (6.4) are compared in Fig. 12. For the present uncertainties (3.14) — the curves in the figure refer to $\xi = 8$ (upper), $D_2 = 0$ in Eq. (2.18) (middle) and $\xi = 12$ (lower) — it is not possible to draw any conclusions from the soft-gluon result. The Padé summation, on the other hand, provides rather definite predictions: The terms beyond α_s^5 can be expected to have a very small impact at $x \lesssim 0.75$. For our standard reference value $\alpha_s = 0.2$ their effect reaches about the size of the N^{4}LO and N^{3}LO contributions at $x \simeq 0.9$ and $x \simeq 0.95$, respectively.

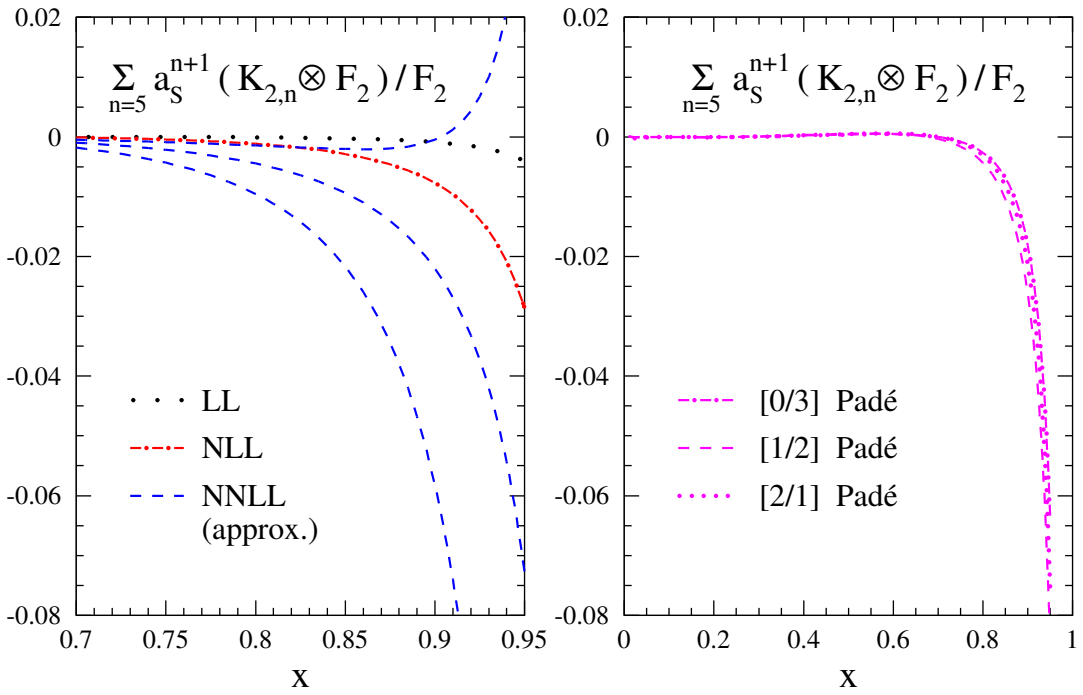

Figure 12: Predictions of the soft-gluon resummation (2.17) and the Padé approximations (6.4) for the contributions beyond N^{4}LO to the logarithmic scale derivative of $F_2 \equiv F_{2,\mathrm{NS}}$.

7 Summary

We have investigated the predictions of massless perturbative QCD for the scaling violations of the most important non-singlet structure functions in unpolarized DIS, extending our previous NNLO results [11] to N^{3}LO and N^{4}LO for the region $x > 10^{-2}$. The main objective of this extension is to reduce the theoretical uncertainty of determinations of α_s from inclusive DIS to about 1%, an accuracy which is sufficient to make full use of present and future structure function measurements. Our results also facilitate improved determinations of power-suppressed contributions to the structure-function evolution by fits to data, especially at large x where the uncertainties are still sizeable at NNLO.

The new ingredients entering the N^{3}LO physical evolution kernels are the four-loop splitting functions and the three-loop coefficient functions. The impact of the former quantities is expected to be very small in the $\overline{\rm MS}$ scheme at $x > 10^{-2}$; it has been estimated by a Padé approximation assigned a 100% uncertainty. For the latter quantities we have derived approximate expressions based on the available integer moment [7, 8] and soft gluon [15, 16] results. The effect of these functions is very well under control at $x > 10^{-2}$, and almost perfectly at $x \gtrsim 0.1$. In fact, the uncertainty of the splitting functions dominates the small residual uncertainties of the evolution kernels. Hence the accuracy of our present N^{3}LO results will be superseded only by a future four-loop calculation.

We have also studied the predictions of the NNLL soft-gluon resummation [17] and of the Padé, PMS and ECH approximations [18, 19, 20]. Presently the predictions of the resummation for the physical evolution kernels beyond N^{3}LO (in any case applicable only at $x \gtrsim 0.8$) suffer from the incomplete determination of the soft-gluon parameters B_2 and D_2, a problem which will be removed by forthcoming exact calculation of the three-loop coefficient functions [33]. The Padé, PMS and ECH approximations are found to agree rather well with the NNLO and N^{3}LO results for the evolution kernels; these approaches seem to provide reliable predictions of the effects at N^{4}LO and beyond.

For $\alpha_s \lesssim 0.2$ the N^{3}LO and N^{4}LO corrections at $\mu_r \simeq Q$ are very small at $x < 0.6$ and $x < 0.8$, respectively, especially for the most accurately measured structure function F_2. Consequently the central values of α_s determined from the non-singlet scaling violations hardly change any more once the larger NNLO terms have been included, see also ref. [3]. The scale uncertainty of the resulting $\alpha_s(M_Z^2)$ is reduced to the unproblematic level of less than 1% at N^{3}LO and 0.5% at N^{4}LO. In order to ensure an overall theoretical accuracy of about 1% also the heavy quark (especially charm) mass effects need to be controlled with this precision. We will address this point in a forthcoming publication.

FORTRAN subroutines of our approximations of the three-loop coefficient functions in section 3 and of the parametrizations of the convolutions entering the evolution kernels in section 4 can be found at `http://www.lorentz.leidenuniv.nl/~avogt`.

Acknowledgment

We are grateful to J. Vermaseren for communicating the fourteenth moment of the three-loop coefficient function for F_2 to us prior to publication. This work has been supported by the European Community TMR research network 'Quantum Chromodynamics and the Deep Structure of Elementary Particles' under contract No. FMRX–CT98–0194.

Appendix: Convolutions of +-distribution

The convolutions $\mathcal{D}_i \otimes \mathcal{D}_j$ of the +-distributions (3.2) for $i + j \leq 4$ are given by

$$
\begin{aligned}
\mathcal{D}_0 \otimes \mathcal{D}_0 &= 2\,\mathcal{D}_1 - \zeta_2\,\delta(1-x) \\
\mathcal{D}_1 \otimes \mathcal{D}_0 &= \frac{3}{2}\,\mathcal{D}_2 - \zeta_2\,\mathcal{D}_0 + \zeta_3\,\delta(1-x) \\
\mathcal{D}_1 \otimes \mathcal{D}_1 &= \mathcal{D}_3 - 2\zeta_2\,\mathcal{D}_1 + 2\zeta_3\,\mathcal{D}_0 - \frac{1}{10}\,\zeta_2^2\,\delta(1-x) \\
\mathcal{D}_2 \otimes \mathcal{D}_0 &= \frac{4}{3}\,\mathcal{D}_3 - 2\zeta_2\,\mathcal{D}_1 + 2\zeta_3\,\mathcal{D}_0 - \frac{4}{5}\,\zeta_2^2\,\delta(1-x) \\
\mathcal{D}_2 \otimes \mathcal{D}_1 &= \frac{5}{6}\,\mathcal{D}_4 - 3\zeta_2\,\mathcal{D}_2 + 6\zeta_3\,\mathcal{D}_1 - \zeta_2^2\,\mathcal{D}_0 + \Big(4\zeta_5 - 2\zeta_2\zeta_3\Big)\,\delta(1-x) \\
\mathcal{D}_2 \otimes \mathcal{D}_2 &= \frac{2}{3}\,\mathcal{D}_5 - 4\zeta_2\,\mathcal{D}_3 + 12\zeta_3\,\mathcal{D}_2 - 4\zeta_2^2\,\mathcal{D}_1 + \Big(16\zeta_5 - 8\zeta_2\zeta_3\Big)\,\mathcal{D}_0 \\
&\quad + \left(4\zeta_3^2 - \frac{46}{35}\,\zeta_2^3\right)\,\delta(1-x) \\
\mathcal{D}_3 \otimes \mathcal{D}_0 &= \frac{5}{4}\,\mathcal{D}_4 - 3\zeta_2\,\mathcal{D}_2 + 6\zeta_3\,\mathcal{D}_1 - \frac{12}{5}\,\zeta_2^2\,\mathcal{D}_0 + 6\zeta_5\,\delta(1-x) \\
\mathcal{D}_3 \otimes \mathcal{D}_1 &= \frac{3}{4}\,\mathcal{D}_5 - 4\zeta_2\,\mathcal{D}_3 + 12\zeta_3\,\mathcal{D}_2 - \frac{27}{5}\,\zeta_2^2\,\mathcal{D}_1 + \Big(18\zeta_5 - 6\zeta_2\zeta_3\Big)\,\mathcal{D}_0 \\
&\quad + \left(3\zeta_3^2 - \frac{36}{35}\,\zeta_2^3\right)\,\delta(1-x) \\
\mathcal{D}_4 \otimes \mathcal{D}_0 &= \frac{6}{5}\,\mathcal{D}_5 - 4\zeta_2\,\mathcal{D}_3 + 12\zeta_3\,\mathcal{D}_2 - \frac{48}{5}\,\zeta_2^2\,\mathcal{D}_1 + 24\zeta_5\,\mathcal{D}_0 - \frac{192}{35}\,\zeta_2^3\,\delta(1-x)
\end{aligned}
\tag{A.1}
$$

up to integrable contributions dealt with numerically in section 4. Here ζ_l stand for the Riemann ζ-function, and ζ_4 and ζ_6 have been expressed in terms of ζ_2 and ζ_3, respectively. A convenient method to derive (and to extend, if required) eqs. (A.1) is by using the relation between $\mathcal{D}_i$ and the harmonic sums discussed, for example, in ref. [34].

References

[1] D.E. Groom et al., Particle Data Group, Eur. Phys. J. **C15** (2000) 1, and refs. therein

[2] W. Furmanski and R. Petronzio, Z. Phys. **C11** (1982) 293

[3] A.L. Kataev, A. Kotikov, G. Parente and A.V. Sidorov, Phys. Lett. **B417** (1998) 374; A.L. Kataev, G. Parente and A.V. Sidorov, Nucl. Phys. **B573** (2000) 405; preprint `hep-ph/0012014` (CERN-TH-2000-343)

[4] J. Santiago and F.J. Yndurain, Nucl. Phys. **B563** (1999) 45; preprint `hep-ph/0102312` (FTUAM 01-01)

[5] E.B. Zijlstra and W.L. van Neerven, Phys. Lett. **B272** (1991) 127; ibid. **B273** (1991) 476; ibid. **B297** (1992) 377; Nucl. Phys. **B383** (1992) 525

[6] S. Moch and J.A.M. Vermaseren, Nucl. Phys. **B573** (2000) 853

[7] S.A. Larin, T. van Ritbergen, and J.A.M. Vermaseren, Nucl. Phys. **B427** (1994) 41; S.A. Larin, P. Nogueira, T. van Ritbergen, and J.A.M. Vermaseren, Nucl. Phys. **B492** (1997) 338

[8] A. Retey and J.A.M. Vermaseren, preprint `hep-ph/0007294` (NIKHEF-2000-018); J.A.M. Vermaseren, private communication

[9] J. A. Gracey, Phys. Lett. **B322** (1994) 141; J.F. Bennett and J.A. Gracey, Nucl. Phys. **B517** (1998) 241

[10] S. Catani and F. Hautmann, Nucl. Phys. **B427** (1994) 475; J. Blümlein and A. Vogt, Phys. Lett. **B370** 1996) 149; V.S. Fadin and L.N. Lipatov, Phys. Lett. **B429** (1998) 127, and refs. therein; M. Ciafaloni and G. Camici, Phys. Lett. **B430** (1998) 349

[11] W.L. van Neerven and A. Vogt, Nucl. Phys. **B568** (2000) 263

[12] W.L. van Neerven and A. Vogt, Nucl. Phys. **B588** (2000) 345

[13] W.L. van Neerven and A. Vogt, Phys. Lett. **B490** (2000) 111

[14] R. Hamberg, W.L. van Neerven and T. Matsuura, Nucl. Phys. **B359** (1991) 343; W.L. van Neerven and E.B. Zijlstra, Nucl. Phys. **B382** (1992) 11

[15] G. Sterman, Nucl. Phys. **B281** (1987) 310; L. Magnea, Nucl. Phys. **B349** (1991) 703; S. Catani and L. Trentadue, Nucl. Phys. **B327** (1989) 323; ibid. **B353** (1991) 183; S. Catani, G. Marchesini and B.R. Webber, Nucl. Phys. **B349** (1991) 635

[16] A. Vogt, Phys. Lett. **B471** (1999) 97

[17] A. Vogt, Phys. Lett. **B497** (2001) 228

[18] M.A. Samuel, J. Ellis and M. Karliner, Phys. Rev. Lett. **74** (1995) 4380;
J. Ellis, E. Gardi, M. Karliner and M.A. Samuel, Phys. Lett. **B366** (1996) 268;
Phys. Rev. **D54** (1996) 6986;
S. J. Brodsky et al., Phys. Rev. **D56** (1997) 6980

[19] P. M. Stevenson, Phys. Rev. **D23** (1981) 2916

[20] G. Grunberg, Phys. Rev. **D29** (1984) 2315

[21] O.V. Tarasov, A.A. Vladimirov, and A.Yu. Zharkov, Phys. Lett. **B93** (1980) 429;
S.A. Larin and J.A.M. Vermaseren, Phys. Lett. **B303** (1993) 334

[22] T. van Ritbergen, J.A.M. Vermaseren and S.A. Larin, Phys. Lett. **B400** (1997) 379

[23] G. Curci, W. Furmanski and R. Petronzio, Nucl. Phys. **B175** (1980) 27

[24] A. Gonzales-Arroyo, C. Lopez and F.J. Yndurain, Nucl. Phys. **B153** (1979) 161;
G. P. Korchemsky, Mod. Phys. Lett. **A4** (1989) 1257;
S. Albino and R.D. Ball, preprint `hep-ph/0011133` (CERN-TH/2000-332)

[25] T. Matsuura and W.L. van Neerven, Z. Phys. **C38** (1988) 623

[26] S. Catani, D. de Florian and M. Grazzini, preprint `hep-ph/0102227` (CERN-TH-2001-044);
R. V. Harlander and W. B. Kilgore, preprint `hep-ph/0102241` (BNL-HET-01-6)

[27] S. Catani, M.L. Mangano, P. Nason and L. Trentadue, Nucl. Phys. **B478** (1996) 273

[28] E. Remiddi and J.A.M. Vermaseren, Int. J. Mod. Phys. **A15** (2000) 725

[29] M. Krämer, E. Laenen and M. Spira, Nucl. Phys. **B511** (1998) 523

[30] M. Diemoz, F. Ferroni, E. Longo and G. Martinelli, Z. Phys. **C39** (1988);
M. Glück, E. Reya and A. Vogt, Z. Phys. **C48** (1990) 471;
Ch. Berger, D. Graudenz, M. Hampel and A. Vogt, Z. Phys. **C70** (1996) 77;
D. A. Kosower, Nucl. Phys. **B506** (1997) 439; ibid. **B520** (1998) 263

[31] A.L. Kataev and V.V. Starshenko, Mod. Phys. Lett. **A10** (1995) 235

[32] D. Redfern, *The Maple Handbook (Maple V release 4)*, Springer 1996

[33] S. Moch and J.A.M. Vermaseren, Nucl. Phys. (Proc. Suppl.) **89** (2000) 131; ibid. 137;
S. Moch, J.A.M. Vermaseren and M. Zhou, in preparation

[34] J. Blümlein and S. Kurth, Phys. Rev. **D60** (1999) 014018